Advances in Nano Research, *Vol. 11, No. 6 (2021) 621-640*
https://doi.org/10.12989/anr.2021.11.6.621

Novel four-unknowns quasi 3D theory for bending, buckling and free vibration of functionally graded carbon nanotubes reinforced composite laminated nanoplates

Adnan I. Khadir[1,2a], Ahmed Amine Daikh[3], Mohamed A. Eltaher*[1,4]

[1]*Faculty of Engineering, Mechanical Engineering Department, King Abdulaziz University, P.O. Box 80204, Jeddah, Saudi Arabia*
[2]*Faculty of Engineering, Mechanical Engineering Department, Jordan University of Science and Technology, P.O. Box 3030, 2011 Irbid, Jordan*
[3]*Laboratoire d'Etude des Structures et de Mécanique des Matériaux, Département de Génie Civil, Faculté des Sciences et de la Technologie, Université Mustapha Stambouli B.P. 305, R.P. 29000 Mascara, Algérie*
[4]*Faculty of Engineering, Mechanical Design and Production Department, Zagazig University, P.O. Box 44519, Zagazig, Egypt*

(*Received May 25, 2021, Revised September 6, 2021, Accepted September 14, 2021*)

Abstract. Effect of thickness stretching on mechanical behavior of functionally graded (FG) carbon nanotubes reinforced composite (CNTRC) laminated nanoplates resting on elastic foundation is analyzed in this paper using a novel quasi 3D higher-order shear deformation theory. The key feature of this theoretical formulation is that, in addition to considering the thickness stretching effect, the number of unknowns of the displacement field is reduced to four, and which is more than five in the other models. Single-walled carbon nanotubes (SWCNTs) are the reinforced elements and are distributed with four power-law functions which are, uniform distribution, V-distribution, O-distribution and X-distribution. To cover various boundary conditions, an analytical solution is developed based on Galerkin method to solve the governing equilibrium equations by considering the nonlocal strain gradient theory. A modified two-dimensional variable Winkler elastic foundation is proposed in this study for the first time. A parametric study is executed to determine the influence of the reinforcement patterns, power-law index, nonlocal parameter, length scale parameter, thickness and aspect ratios, elastic foundation, thermal environments, and various boundary conditions on stresses, displacements, buckling loads and frequencies of the CNTRC laminated nanoplate.
Keywords: bending; buckling; free vibration; galerkin method; nonlocal strain gradient theory; quasi 3D shear deformation theory; variable Winkler elastic foundation

1. Introduction

Nowadays, Carbon nanotubes (CNTs) are considered as "new materials for the twenty-first century" (Harris 2004). CNTs serve as an excellent reinforcement for the composite structures due to their remarkable mechanical, electrical, and thermal characteristics such as high tensile modulus, high strength, low density and can sustain large elastic strain (Esawi and Farag 2007). Exceptional mechanical properties of FGM and CNTs may be obtained together through functionally graded distribution of CNTs (Duk *et al*. 2017, Shen 2009). This proper combination of CNTs and FGM concept was first introduced by Shen (Shen 2009) studying the nonlinear bending behavior of functionally graded carbon nanotube reinforced composites (FG-CNTRC) plates.

Due to the vigorous development in nanotechnology, the engineering nanostructures such as nanorods, nanobeams and nanoplates have been growing in numerous modern engineering industries (Ekinci and Roukes 2005). Among the application of nanostructures can be referred to micro/nano electro-mechanical systems (MEMS/NEMS), nanocomposite and nano actuators. In these applications, size effects become very prominent. Therefore, the inclusion of the size effects in the analysis of the mechanical behavior of these nanostructures is very necessary for better designing or understanding these small-scaled structures. It should be noted that classical continuum mechanics theory is not suitable for nanostructures due to neglecting size influence in nanosize structures. To overcome this problem, various non-classical continuum theories imply additional material length scale parameters were developed, such as nonlocal elasticity theory proposed via Eringen (1972, 1983), strain gradient theory (SGT) (Yang *et al*. 2002), modified couple stress theory (MCST) (Yang *et al*. 2002), surface elasticity theory (Gurtin and Murdooh 1978) and nonlocal strain gradient theory (NSGT) (Askes and Aifantis 2009, She *et al*. 2018, Daikh *et al*. 2020a).

However, the studies of size-dependence effects on the mechanical behavior of FG elastic materials with micro/nanostructure should be related to both internal lengths and external dimensions and are always of fundamental significance. In contrast to classical elasticity theory, the stress of nonlocal elasticity theory at a reference point accounts for not only the strain at the reference point, but also the strains at all points in the whole body.

With the increasing application of FGM nanostructures,

*Corresponding author, Ph.D. Student,
E-mail: meltaher@kau.edu.sa; mohaeltaher@gmail.com
[a] Ph.D., E-mail: akhdair@kau.edu.sa; akhdair@just.edu.jo

ISSN: 2287-237X (Print), 2287-2388 (Online)

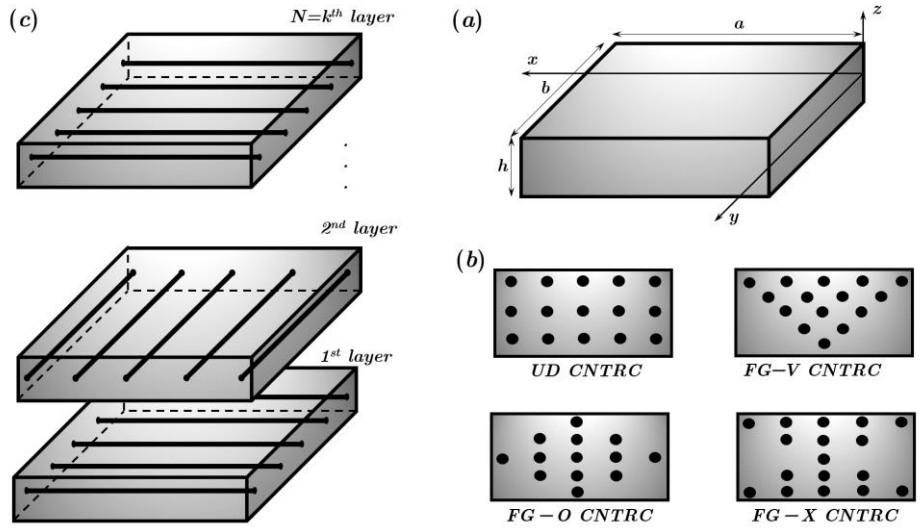

Fig 1. Geometry and cross-sections of FG-CNTRC laminated nanoplate

understanding their responses becomes an important task. In the literature, three main theories have been proposed to analyze accurately the behavior of FGM nanostructures. The classical plate theory (CPT), based on Kirchhoff's assumptions, ignoring the transverse shear strain is suitable only for thin plates/shells (Chi and Chung 2006). However, it is not appropriate for the moderately thick and thick plates, which require that the transverse shear and normal strains should be considered. The next class of theory, known as first-order shear deformation theory (FSDT) which considers constant transverse shear stresses through the plate thickness (Nguyen *et al.* 2019, Bekhadda *et al.* 2019, Zenkour 2016). However, it needs a shear correction factor whose value depends on several factors such as end condition, thickness scheme, material properties, etc. (Mantari and Ore 2015). To overcome the drawbacks of CPT and FSDT, various higher-order shear deformation theories (HSDT) were developed for a better representation of transverse shear stresses without the use of correction factors (Ferreira *et al.* 2009, Neves *et al.* 2013, Thai *et al.* 2014, 2016, Houari *et al.* 2013, Belarbi *et al.* 2020, 2021 Daikh *et al.* 2020b, Davood *et al.* 2018, Bensaid 2017, Husaain 2020a, b, Nguyen *et al.* 2017). Thermal behavior analysis of (FG) of sandwich nanoplates was analytically investigated to highlight the effect of temperature on the material properties (Daikh 2019, 2020, Davood *et al.* 2018, Daikh and Megueni 2017, Daikh *et al.* 2019a, b, 2020b, c, g, Pham *et al.* 2020). They found that the material properties of the FGM layers depend on temperature and degrade continuously through the thickness direction. Static and bending analyses of FG sandwich nanoplates at various boundary conditions were analyzed under different distributions functions to study the impact of material distribution, sandwich nanoplate geometry, boundary conditions and elastic parameters on stresses and deflections of FG sandwich nanoplates (Vaghefi 2020, Daikh *et al.* 2020d, e, Hamed *et al.* 2020, Daikh and Zenkour 2020). Dynamic, vibration, stability problems and frequency parameters of the nanostructures of FG sandwiches were investigated by many researchers (Cao *et al.* 2021, Esen *et al.* 2020, 2021, Jena *et al.* 2019, Al-Furjan 2019, Pham *et al.* 2021, Liew and Alibeigloo 2020, Ehyaei *et al.* 2017, Eltaher *et al.* 2016, Ebrahimi and Barati 2016, Bensaid *et al.* 2020, Esen *et al.* 2021).

The study aims to find out the mechanical response of FG-CNTRC plates using simple and efficient formulations. A new Qausi 3D HSDT is proposed to fulfill both parabolic shear distribution through the thickness and the zero-shear at free boundaries. In the literature, the analytical solutions are performed based on Navier's technique, which is related to the simply supported boundary conditions. For this purpose, a simple analytical solution is developed based on Galerkin method to cover the different boundary conditions considering the thickness stretching effect. The proposed model is limited to uniform cross-sectional and straight FG-CNTRC nanoplates. The developed analytical model is compared with other available theories in the literature. A modified two-dimensional variable Winkler elastic foundation is proposed in the present work. The influence of CNTs patterns on the structure response and mechanical behavior is to be confirmed and the effect of size dependency and various boundary conditions is investigated.

2. Formulation

2.1 Material distribution functions

Consider a laminated nanoplate of length (a), width (b) and thickness (h) as shown in Fig. 1. All nanoplate layers have the same thickness and are made from polymer matrix and reinforced by CNTs. Three different functionally graded distributions of CNTs reinforcement along the thickness of the nanoplate layers are presented in this work based on power-law index (Fig. 2), in addition to the uniform distribution (UD) CNTs distribution.

Volume fraction of CNTs of each sheet for various patterns, is expressed as

FG─X CNTRC laminated nanoplate:

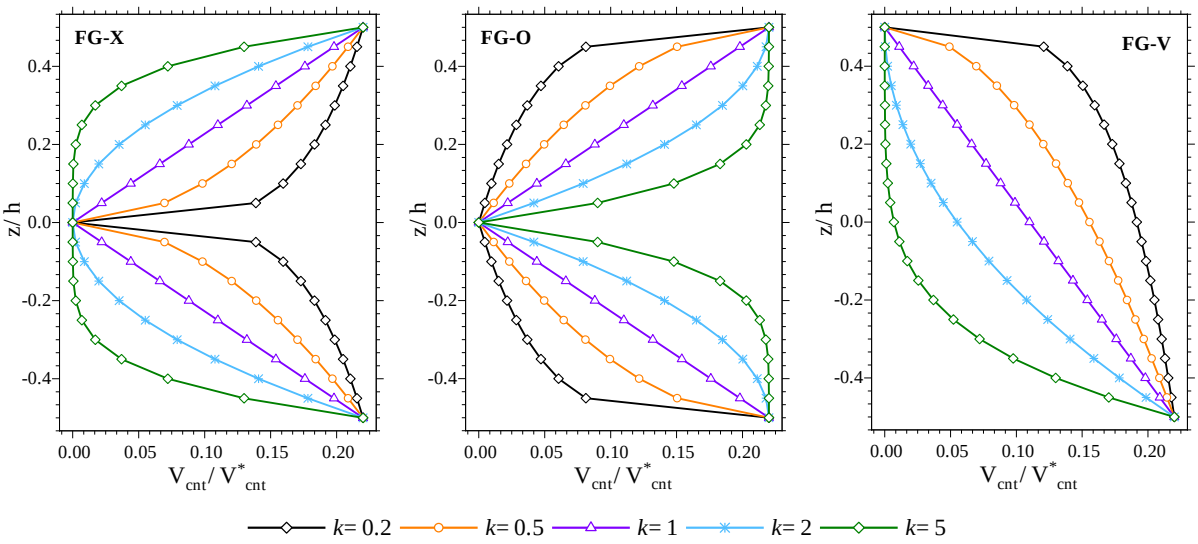

Fig. 2 Variation of CNTs volume fraction for various power-law index; (a): X-distribution, (b): O-distribution, (c): V-distribution

$$V_{cnt} = 2\left(\frac{\left|2|z| - \left|z_{(k-1)} + z_{(k)}\right|\right|}{z_{(k)} - z_{(k-1)}}\right)^{k} V^{*}_{cnt} \tag{1}$$

FG—O CNTRC laminated nanoplate:

$$V_{cnt} = 2\left(1 - \left(\frac{\left|2|z| - \left|z_{(k-1)} + z_{(k)}\right|\right|}{z_{(k)} - z_{(k-1)}}\right)^{k}\right) V^{*}_{cnt} \tag{2}$$

FG—V CNTRC laminated nanoplate:

$$V_{cnt} = 2\left(\frac{1}{2} - \left(\frac{2z - z_{(k)} - z_{(k-1)}}{2\left(z_{(k)} - z_{(k-1)}\right)}\right)\right)^{k} V^{*}_{cnt} \tag{3}$$

UD CNTRC laminated nanoplate:

$$V_{cnt} = V^{*}_{cnt} \tag{4}$$

where k is power-law index and V^{*}_{cnt} is the total volume fraction of CNTs, which can be calculated from the following equation

$$V^{*}_{cnt} = \frac{W_{cnt}}{W_{cnt} + (\rho_{cnt}/\rho_{m})(1 - W_{cnt})} \tag{5}$$

where W_{cnt} is the CNTs mass fraction, ρ_{CNT} is the CNTs mass density and ρ_{m} is polymer matrix mass density. The effective Young's modulus and shear modulus of the CNTRC laminated nanoplates are defined using the extended rule of mixture and the molecular dynamics simulations and given by (Han and Elliott 2007)

$$E^{k}_{11} = \eta_1 V_{cnt} E^{cnt}_{11} + V_p E_p, \quad \frac{\eta_2}{E^{k}_{22}} = \frac{V_{cnt}}{E^{cnt}_{22}} + \frac{V_p}{E_p}, \quad \frac{\eta_3}{G^{k}_{12}} = \frac{V_{cnt}}{G^{cnt}_{12}} + \frac{V_p}{G_p} \tag{6}$$

E^{k}_{11} and E^{k}_{22} are Young's moduli in x-direction and y-direction, and G^{k}_{12} is the shear modulus. The subscripts p and cnt refer to the properties of the matrix and the CNTs. The parameters η_i $(i = 1,2,3)$ are efficiency parameters of the CNTs where $\eta_1 = 0.149$, $\eta_2 = \eta_3 = 0.934$, for the case of $V^{*}_{cnt} = 0.11$, $\eta_1 = 0.150$, $\eta_2 = \eta_3 = 0.941$, for the case of $V^{*}_{cnt} = 0.14$ and $\eta_1 = 0.149$, $\eta_2 = \eta_3 = 1.381$, for the case of $V^{*}_{cnt} = 0.17$ (Daikh *et al.* 2020f).

The volume fraction of the polymer V_p is related to CNT volume fraction V_{cnt} by the relation:

$$V_{cnt} + V_p = 1 \tag{7}$$

Poisson's ratio ν_{12}, mass density ρ, thermal expansion coefficients in the longitudinal and transverse directions, α_{11} and α_{22} of k layer can be computed by (Shen 2009)

$$\nu_{12} = V_{cnt}\nu^{cnt}_{12} + V_p\nu_p \tag{8}$$

$$\rho = V_{cnt}\rho_{cnt} + V_p\rho_p \tag{9}$$

$$\alpha_{11} = V_{cnt}\alpha^{cnt}_{11} + V_p\alpha_p \tag{10}$$

$$\alpha_{22} = (1 + \nu^{cnt}_{12})V_{cnt}\alpha^{cnt}_{22} + (1 + \nu_p)V_p\alpha_p - \nu_{12}\alpha_{11} \tag{11}$$

The other effective mechanical properties of mixture of CNTs and matrix isotropic polymer are

$$E_{33} = E_{22}, \quad G_{12} = G_{13} = G_{23}, \quad \nu_{13} = \nu_{12}, \quad \nu_{31} = \nu_{21}, \quad \nu_{32} = \nu_{23} = \nu_{21}, \quad \nu_{21} = \frac{E_{22}}{E_{11}}\nu_{12}$$

2.2 Nonlocal strain gradient theory

Lim *et al* (2015) developed a function of stresses by considering the strain gradient stress and nonlocal elastic stress fields which can be written as:

$$\sigma_{ij} = \sigma^{(0)}_{ij} - \frac{d\sigma^{(1)}_{ij}}{dx} \tag{12}$$

where $\sigma_{ij}^{(0)}$ and $\sigma_{ij}^{(1)}$ are the stresses corresponds to strain ε_{kl} and strain gradient $\varepsilon_{kl,x}$, and can be expressed in the form

$$\begin{aligned}\sigma_{ij}^{(0)} &= \int_0^L C_{ijkl}\alpha_0(x,x',e_0a)\varepsilon_{kl,x}(x')dx' \\ \sigma_{ij}^{(1)} &= l^2\int_0^L C_{ijkl}\alpha_1(x,x',e_1a)\nabla\varepsilon_{kl,x}(x')dx'\end{aligned} \tag{13}$$

C_{ijkl} is the elastic constant, e_0a and e_1a are the nonlocal parameters and l is the strain gradient parameter. $\alpha_0(x,x',e_0a)$ and $\alpha_1(x,x',e_1a)$ are the nonlocal kernel functions (Eringen 1983). The constitutive relation of nonlocal strain gradient theory can be written as

$$\begin{aligned}[1-(e_1a)^2\nabla^2][1-(e_0a)^2\nabla^2]\sigma_{ij} \\ = C_{ijkl}[1-(e_1a)^2\nabla^2]\varepsilon_{kl} \\ - C_{ijkl}l^2[1-(e_0a)^2\nabla^2]\nabla^2\varepsilon_{kl}\end{aligned} \tag{14}$$

∇^2 denotes the Laplacian operator. By assuming that the coefficient $e = e_0 = e_1$, The total constitutive relation takes the following form

$$[1-\mu\nabla^2]\sigma_{ij} = C_{ijkl}[1-\lambda\nabla^2]\varepsilon_{kl} \tag{15}$$

where $\mu = (ea)^2$ and $\lambda = l^2$.

2.3 Displacement field

The new proposed mathematical model is built upon the classical plate theory (CPT) including the effect of transverse normal stress. The proposed model has four unknowns, which is even less than the other quasi-3D theories with five or more unknowns. The displacement field can be represented in terms of generalized transverse shear strain function $f(z)$ as (Houari *et al*. 2016):

$$\begin{aligned}u(x,y,z,t) &= u_0 - z\frac{\partial w_0}{\partial x} - \beta f(z)\frac{\partial^3 w_0}{\partial x^3} \\ v(x,y,z,t) &= v_0 - z\frac{\partial w_0}{\partial y} - \beta f(z)\frac{\partial^3 w_0}{\partial y^3} \\ w(x,y,z,t) &= w_0 + \beta\, g(z)\,\psi_z\end{aligned} \tag{16}$$

Here, u_0, v_0, and w_0 are the displacement at midplane of the plate. The additional displacement ψ_z accounts for transverse normal stress effect, and the shape function f(z) represents the distribution of the transverse shear strains and shear stresses. In the present work, we propose a new hyperbolic sine function shear deformation theory which is given as

$$f(z) = h\sinh\left(\frac{z}{h}\right) - \frac{3z^3}{2h^2} \tag{17a}$$

where h is the total laminate thickness and $g(z)$ can be evaluated by

$$g(z) = f'(z) = \frac{df(z)}{dz} \tag{17b}$$

For comparison, Fig. 3 illustrates the shape functions $f(z)$ and first derivatives f'(z) of typical transverse shear functions based on the third order shear deformation theory "TSDT" of Reddy (1984) and the sinusoidal shear deformation theory "SSDT" of Touratier (1991).

Based on the displacement field relations given in Eq. (16), the nonzero strains can be evaluated by

$$\begin{aligned}\begin{Bmatrix}\varepsilon_{xx}\\ \varepsilon_{yy}\\ \gamma_{xy}\end{Bmatrix} &= \begin{bmatrix}\varepsilon_{xx}^{(0)} & \varepsilon_{xx}^{(1)} & \varepsilon_{xx}^{(2)}\\ \varepsilon_{yy}^{(0)} & \varepsilon_{yy}^{(1)} & \varepsilon_{yy}^{(2)}\\ \gamma_{xy}^{(0)} & \gamma_{xy}^{(1)} & \gamma_{xy}^{(2)}\end{bmatrix}\begin{Bmatrix}1\\ z\\ f(z)\end{Bmatrix}, \\ \begin{Bmatrix}\gamma_{yz}\\ \gamma_{xz}\end{Bmatrix} &= \beta g(z)\begin{Bmatrix}\gamma_{yz}^0\\ \gamma_{xz}^0\end{Bmatrix}, \quad \varepsilon_{zz} = \beta g'(z)\varepsilon_{zz}^0\end{aligned} \tag{18}$$

where

$$\begin{aligned}\begin{Bmatrix}\varepsilon_{xx}^{(0)}\\ \varepsilon_{yy}^{(0)}\\ \gamma_{xy}^{(0)}\end{Bmatrix} &= \begin{Bmatrix}\dfrac{\partial u_0}{\partial x}\\ \dfrac{\partial v_0}{\partial y}\\ \dfrac{\partial v_0}{\partial x}+\dfrac{\partial u_0}{\partial y}\end{Bmatrix}, \quad \begin{Bmatrix}\varepsilon_{xx}^{(1)}\\ \varepsilon_{yy}^{(1)}\\ \gamma_{xy}^{(1)}\end{Bmatrix} = -\begin{Bmatrix}\dfrac{\partial^2 w_0}{\partial x^2}\\ \dfrac{\partial^2 w_0}{\partial y^2}\\ 2\dfrac{\partial^2 w_0}{\partial x\partial y}\end{Bmatrix}, \\ \begin{Bmatrix}\varepsilon_{xx}^{(2)}\\ \varepsilon_{yy}^{(2)}\\ \gamma_{xy}^{(2)}\end{Bmatrix} &= -\begin{Bmatrix}\dfrac{\partial^4 w_0}{\partial x^4}\\ \dfrac{\partial^4 w_0}{\partial y^4}\\ \dfrac{\partial(\nabla^2 w_0)}{\partial x\partial y}\end{Bmatrix}, \begin{Bmatrix}\gamma_{xz}^{(0)}\\ \gamma_{yz}^{(0)}\end{Bmatrix} = \begin{Bmatrix}-\dfrac{\partial^3 w_0}{\partial x^3}+\dfrac{\partial\psi_z}{\partial x}\\ -\dfrac{\partial^3 w_0}{\partial y^3}+\dfrac{\partial\psi_z}{\partial y}\end{Bmatrix}, \\ \varepsilon_{zz}^{(0)} &= \psi_z,\ \nabla^2 w_0 = \frac{\partial^2 w_0}{\partial x^2}+\frac{\partial^2 w_0}{\partial y^2}\end{aligned} \tag{19}$$

Based on nonlocal strain gradient nanoplate theory, the constitutive stress-strain relations of a kth layer can be written as

$$\begin{aligned}&[1-\mu\nabla^2]\begin{Bmatrix}\sigma_{xx}\\ \sigma_{yy}\\ \sigma_{zz}\\ \tau_{yz}\\ \tau_{xz}\\ \tau_{xy}\end{Bmatrix}^{(k)} \\ &= [1-\lambda\nabla^2]\begin{bmatrix}\bar{Q}_{11}^k & \bar{Q}_{12}^k & \bar{Q}_{13}^k & 0 & 0 & 0\\ \bar{Q}_{12}^k & \bar{Q}_{22}^k & \bar{Q}_{23}^k & 0 & 0 & 0\\ \bar{Q}_{13}^k & \bar{Q}_{23}^k & \bar{Q}_{33}^k & 0 & 0 & 0\\ 0 & 0 & 0 & \bar{Q}_{44}^k & 0 & 0\\ 0 & 0 & 0 & 0 & \bar{Q}_{55}^k & 0\\ 0 & 0 & 0 & 0 & 0 & \bar{Q}_{66}^k\end{bmatrix}\begin{Bmatrix}\varepsilon_{xx}\\ \varepsilon_{yy}\\ \varepsilon_{zz}\\ \gamma_{yz}\\ \gamma_{xz}\\ \gamma_{xy}\end{Bmatrix}^{(k)}\end{aligned} \tag{20}$$

The transformed material constants $\bar{Q}_{ij}^k$ are expressed as:

$$\begin{aligned}\bar{Q}_{11}^k &= Q_{11}cos^4\theta_k + 2(Q_{12}+2Q_{66})sin^2\theta_k cos^2\theta_k \\ &\quad + Q_{22}sin^4\theta_k \\ \bar{Q}_{12}^k &= (Q_{11}+Q_{22}-4Q_{66})sin^2\theta_k cos^2\theta_k \\ &\quad + Q_{12}(sin^4\theta_k + cos^4\theta_k) \\ \bar{Q}_{13}^k &= Q_{13}cos^2\theta_k + Q_{23}sin^2\theta_k \\ \bar{Q}_{22}^k &= Q_{11}sin^4\theta_k + 2(Q_{12}+2Q_{66})sin^2\theta_k cos^2\theta_k \\ &\quad + Q_{22}cos^4\theta_k \\ \bar{Q}_{23}^k &= Q_{13}sin^2\theta_k + Q_{23}cos^2\theta_k \\ \bar{Q}_{66}^k &= (Q_{11}+Q_{22}-2Q_{12}-2Q_{66})sin^2\theta_k cos^2\theta_k \\ &\quad + Q_{66}(sin^4\theta_k + cos^4\theta_k) \\ \bar{Q}_{44}^k &= Q_{44}cos^2\theta_k + Q_{55}sin^2\theta_k \\ \bar{Q}_{55}^k &= Q_{55}cos^2\theta_k + Q_{44}sin^2\theta_k\end{aligned} \tag{21}$$

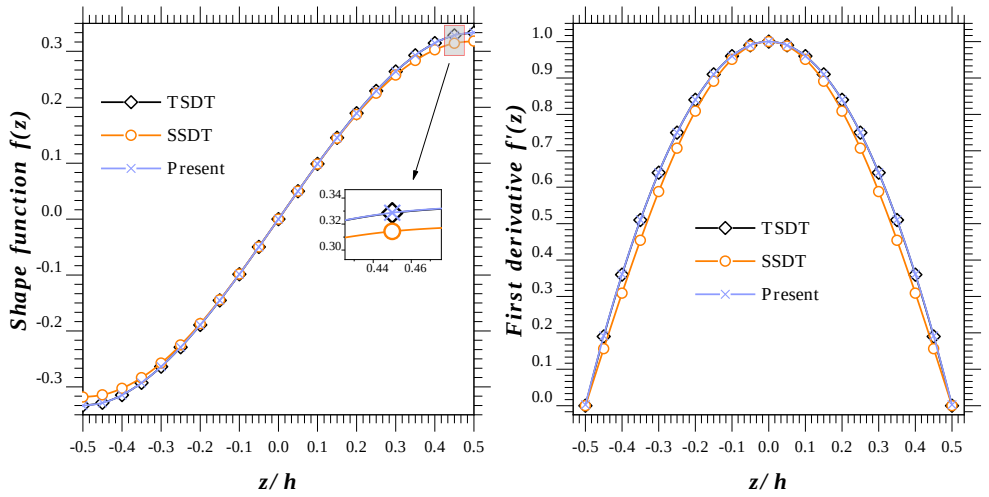

Fig. 3 Variation of shape functions f (z) and its derivative

Here, θ_k denotes the layer's angle.

As the normal strain in z-direction can be discarded (non-stretching), therefore, $\varepsilon_{zz}^{(0)} = 0$, and hence

$$Q_{11} = \frac{E_{11}}{1-\nu_{12}\nu_{21}},\ Q_{22} = \frac{E_{22}}{1-\nu_{12}\nu_{21}},\ Q_{12} = \frac{\nu_{12}E_{22}}{1-\nu_{12}\nu_{21}},\quad Q_{44} = G_{23},\quad Q_{55} = G_{13},\quad Q_{66} = G_{12} \tag{22}$$

However, by considering the stretching through the thickness $(\varepsilon_{zz}^{(0)} \neq 0)$, then Q_{ij} are the 3D elastic constants:

$$\begin{aligned} &Q_{11} = \frac{E_{11}}{\Delta}(1-\nu_{23}\nu_{32}),\quad Q_{22} = \frac{E_{22}}{\Delta}(1-\nu_{31}\nu_{13}),\\ &Q_{33} = \frac{E_{33}}{\Delta}(1-\nu_{12}\nu_{21})Q_{44} = G_{23},\\ &Q_{55} = G_{13},\quad Q_{66} = G_{12}Q_{12} = \frac{E_{11}}{\Delta}(\nu_{21}+\nu_{31}\nu_{23}),\\ &Q_{13} = \tfrac{E_{11}}{\Delta}(\nu_{31}+\nu_{21}\nu_{32}),\quad Q_{23} = \tfrac{E_{22}}{\Delta}(\nu_{32}+\nu_{12}\nu_{31})\\ &\Delta = 1-\nu_{12}\nu_{21}-\nu_{23}\nu_{32}-\nu_{31}\nu_{13}-2\nu_{12}\nu_{32}\nu_{13} \end{aligned} \tag{23}$$

2.4 Variational statements

The Hamilton's principle is used to derive the equations of motion of the CNTRC laminated nanoplate:

$$\int_{t_1}^{t_2} \delta(U-T+V)dt = 0 \tag{24}$$

where U, T and V are the strain energy, the kinetic energy and the virtual work done by external forces, respectively.

The virtual strain energy of the nanoplate can be expressed as

$$\delta U = \int_V \sigma_{ij}{}^{(k)}\delta\varepsilon_{ij}\mathrm{d}V \tag{25}$$

$$= \int_\Omega \begin{bmatrix} N_{xx}\frac{\partial\delta u_0}{\partial x} - M_{xx}\frac{\partial^2\delta w_0}{\partial x^2} - \beta S_{xx}\frac{\partial^4\delta w_0}{\partial x^4} + N_{yy}\frac{\partial\delta v_0}{\partial y} \\ -M_{yy}\frac{\partial^2\delta w_0}{\partial y^2} - \beta S_{yy}\frac{\partial^4\delta w_0}{\partial y^4} + \beta Q_{zz}\delta\psi_z + N_{xy}\left(\frac{\partial\delta u_0}{\partial y}+\frac{\partial\delta v_0}{\partial x}\right) \\ -2M_{xy}\frac{\partial^2\delta w_0}{\partial x\partial y} - \beta S_{xy}\left(\frac{\partial^4\delta w_0}{\partial x^3\partial y}+\frac{\partial^4\delta w_0}{\partial x\partial y^3}\right) + \beta R_{yz}\frac{\partial\delta\psi_z}{\partial y} \\ -\beta R_{yz}\frac{\partial^3\delta w_0}{\partial y^3} + +\beta R_{xz}\frac{\partial\delta\psi_z}{\partial x} - R_{xz}\frac{\partial^3\delta w_0}{\partial x^3} \end{bmatrix}\mathrm{d}x\mathrm{d}y \tag{26}$$

The stress resultants N_{ij}, the stress couples M_{ij}, the additional stress couples S_{ij}, the transverse shear stress resultants R_{iz} and the additional stress couples Q_{zz} associated with transverse normal deformation effect can be defined by:

$$\begin{aligned} \{N_{ij}, M_{ij}, S_{ij}\} &= \sum_{k=1}^{k=n}\int_{h_{k-1}}^{h_k}\{1, z, f(z)\}\sigma_{ij}\mathrm{d}z,\quad i,j = x,y\\ R_{iz} &= \sum_{k=1}^{k=n}\int_{h_{k-1}}^{h_k} g(z)\sigma_{iz}\mathrm{d}z,\quad i,j = x,y\\ Q_{zz} &= \sum_{k=1}^{k=n}\int_{h_{k-1}}^{h_k} g'(z)\sigma_{zz}\mathrm{d}z \end{aligned} \tag{27}$$

By including the effect of in-plane compressive loadings $\bar{N}_{xx}^0 = \chi_1 N_{cr}$ and $\bar{N}_{yy}^0 = \chi_2 N_{cr}$, where χ_1 and χ_2 are the buckling loads intensity, transverse loading q and the variable Winkler elastic foundation f_e, the virtual work can be stated as

$$\begin{aligned} \delta V = &-\int_A (q-f_e)\delta w\mathrm{d}A\\ &+\int_A\left[\bar{N}_{xx}^0\frac{\partial w}{\partial x}\frac{\partial\delta w}{\partial x} + \bar{N}_{yy}^0\frac{\partial w}{\partial y}\frac{\partial\delta w}{\partial y}\right]\mathrm{d}A \end{aligned} \tag{28}$$

where

$$f_e = k_w(w_0 + g(z)\psi_z) \tag{29}$$

where k_w denote the modulus of subgrade reaction (elastic coefficient of Winkler foundation). The proposed Winkler foundation varies through x and y directions based on two parameters κ and ξ (Fig. 4):

$$k_w = \kappa + \xi\begin{cases} \sin\left(\frac{\pi x}{a}\right)\sin\left(\frac{\pi y}{b}\right) & \text{Sinusoidal}\\ 1-\sin\left(\frac{\pi x}{a}\right)\sin\left(\frac{\pi y}{b}\right) & \text{Reverse Sinusoidal}\\ \left(\frac{xy}{ab}\right)^2 & \text{Parabolic}\\ 1-\left(\frac{xy}{ab}\right)^2 & \text{Reverse Parabolic} \end{cases} \tag{30}$$

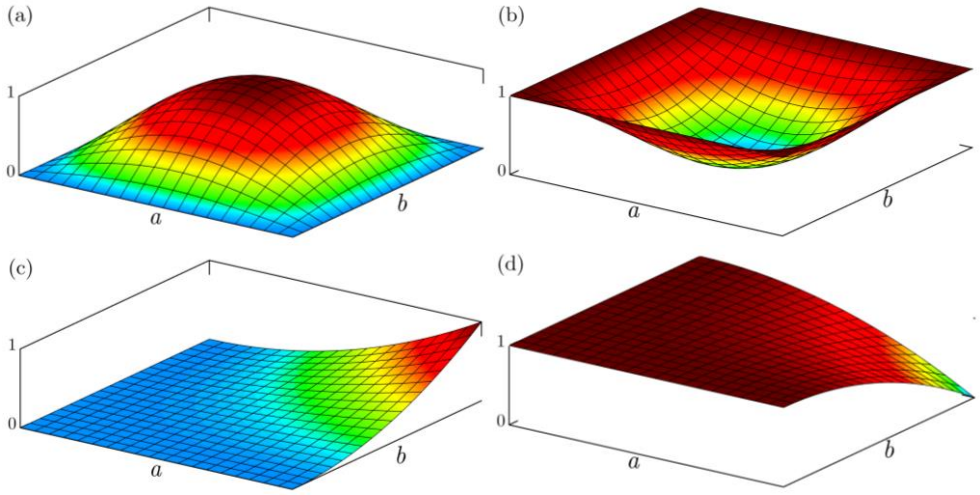

Fig. 4 Winkler elastic foundation intensity (κ = 0, ξ = 1); (a): Sinusoidal, (b): Reverse sinusoidal, (c): Parabolic, (d): Reverse parabolic

The variation of kinetic energy can be expressed by

$$\delta K = \int_V [\dot{u}\delta\dot{u} + \dot{v}\delta\dot{v} + \dot{w}\delta\dot{w}]\mathrm{d}x\mathrm{d}y\mathrm{d}z \tag{31}$$

$$\begin{aligned}
&= \int_A \Bigg\{ I_0(\dot{u}_0\delta\dot{u}_0 + \dot{v}_0\delta\dot{v}_0 + \dot{w}_0\delta\dot{w}_0) \\
&-I_1\left(\frac{\partial\dot{w}_0}{\partial x}\delta\dot{u}_0 + \frac{\partial\dot{w}_0}{\partial y}\delta\dot{v}_0 + \dot{u}_0\frac{\partial\delta\dot{w}_0}{\partial x} + \dot{v}_0\frac{\partial\delta\dot{w}_0}{\partial y}\right) \\
&-\beta I_3\left(\dot{u}_0\frac{\partial^3\delta\dot{w}_0}{\partial x^3} + \frac{\partial^3\dot{w}_0}{\partial x^3}\delta\dot{u}_0 + \dot{v}_0\frac{\partial^3\delta\dot{w}_0}{\partial y^3} + \frac{\partial^3\dot{w}_0}{\partial y^3}\delta\dot{v}_0\right) \\
&+I_2\left(\frac{\partial\dot{w}_0}{\partial x}\frac{\partial\delta\dot{w}_0}{\partial x} + \frac{\partial\dot{w}_0}{\partial y}\frac{\partial\delta\dot{w}_0}{\partial y}\right) \\
&+\beta I_4\left(\frac{\partial\dot{w}_0}{\partial x}\frac{\partial^3\delta\dot{w}_0}{\partial x^3} + \frac{\partial^3\dot{w}_0}{\partial x^3}\frac{\partial\delta\dot{w}_0}{\partial x} + \frac{\partial\dot{w}_0}{\partial y}\frac{\partial^3\delta\dot{w}_0}{\partial y^3} + \frac{\partial^3\dot{w}_0}{\partial y^3}\frac{\partial\delta\dot{w}_0}{\partial y}\right) \\
&+\beta^2 I_5\left(\frac{\partial^3\dot{w}_0}{\partial x^3}\frac{\partial^3\delta\dot{w}_0}{\partial x^3} + \frac{\partial^3\dot{w}_0}{\partial y^3}\frac{\partial^3\delta\dot{w}_0}{\partial y^3}\right) \\
&+\beta J_0(\dot{\varphi}_z\delta\dot{w}_0 + \dot{w}_0\delta\dot{\varphi}_z) + \beta^2 J_1(\dot{\varphi}_z\delta\dot{\varphi}_z)\Bigg\}\mathrm{d}x\mathrm{d}y\mathrm{d}z
\end{aligned} \tag{32}$$

where

$$\begin{aligned}
&\{I_0, I_1, I_2, I_3, I_4, I_5\} \\
&= \sum_{k=1}^{k=n}\int_{-h/2}^{h/2}\rho^{(k)}(z)\left\{1, z, z^2, \mathrm{f}(z), zf(z), \left(f(z)\right)^2\right\}\mathrm{d}z \\
&\{J_0, J_1\} = \sum_{k=1}^{k=n}\int_{-h/2}^{h/2}\rho^{(k)}(z)\left\{g(z), \left(g(z)\right)^2\right\}\mathrm{d}z
\end{aligned} \tag{33}$$

Therefore, the equations of motion of the nanoplate can be described by

$$\begin{aligned}
&\delta u_0: \frac{\partial N_{xx}}{\partial x} + \frac{\partial N_{xy}}{\partial y} = I_0\ddot{u}_0 - I_1\frac{\partial\ddot{w}_0}{\partial x} - I_3\beta\frac{\partial^3\ddot{w}_0}{\partial x^3} \\
&\delta v_0: \frac{\partial N_{xy}}{\partial x} + \frac{\partial N_{yy}}{\partial y} = I_0\ddot{v}_0 - I_1\frac{\partial\ddot{w}_0}{\partial y} - I_3\beta\frac{\partial^3\ddot{w}_0}{\partial y^3} \\
&\delta w_0: \frac{\partial^2 M_{xx}}{\partial x^2} + 2\frac{\partial^2 M_{xy}}{\partial x\partial y} + \frac{\partial^2 M_{yy}}{\partial y^2} \\
&+\beta\left(\frac{\partial^4 S_{xx}}{\partial x^4} + \frac{\partial^4 S_{xx}}{\partial y^4} + \frac{\partial^4 S_{xy}}{\partial x^3\partial y} + \frac{\partial^4 S_{xy}}{\partial x\partial y^3} - \frac{\partial^3 R_{yz}}{\partial y^3} - \frac{\partial^3 R_{xz}}{\partial x^3}\right)
\end{aligned} \tag{34}$$

$$\begin{aligned}
&+q - f_e + \bar{N}_{xx}^0\frac{\partial^2 w_0}{\partial x^2} + \bar{N}_{yy}^0\frac{\partial^2 w_0}{\partial y^2} \\
&= I_0\ddot{w}_0 + I_1\left(\frac{\partial\ddot{u}_0}{\partial x} + \frac{\partial\ddot{v}_0}{\partial y}\right) - I_2\left(\frac{\partial^2\ddot{w}_0}{\partial x^2} + \frac{\partial^2\ddot{w}_0}{\partial y^2}\right) \\
&+\beta I_3\left(\frac{\partial^3\ddot{u}_0}{\partial x^3} + \frac{\partial^3 v}{\partial y^3}\right) - 2\beta I_4\left(\frac{\partial^4\ddot{w}_0}{\partial x^4} + \frac{\partial^4\ddot{w}_0}{\partial y^4}\right) \\
&-\beta^2 I_5\left(\frac{\partial^6\ddot{w}_0}{\partial x^6} + \frac{\partial^6\ddot{w}_0}{\partial y^6}\right) + \beta J_0\ddot{\psi}_z \\
&\delta\psi_z: \beta\begin{pmatrix}\dfrac{\partial R_{xz}}{\partial x} + \dfrac{\partial R_{yz}}{\partial y} - Q_{zz} \\ +\mathrm{g}(z)\left(q - f_e + \bar{N}_{xx}^0\dfrac{\partial^2\ddot{\psi}_z}{\partial x^2} + \bar{N}_{yy}^0\dfrac{\partial^2\ddot{\psi}_z}{\partial y^2}\right)\end{pmatrix} \\
&= \beta J_0\ddot{w}_0 + \beta^2 J_1\ddot{\psi}_z
\end{aligned} \tag{34}$$

By the integration of the stress field indicated in Eq. (20), one obtains

$$[1-\mu\nabla^2]\begin{Bmatrix}N_{xx}\\N_{yy}\\N_{xy}\\M_{xx}\\M_{yy}\\M_{xy}\\S_{xx}\\S_{yy}\\S_{xy}\\Q_{zz}\end{Bmatrix} = [1-\lambda\nabla^2]$$

$$\begin{bmatrix}
A_{11} & A_{12} & 0 & B_{11} & B_{12} & 0 & \beta C_{11} & \beta C_{12} & 0 & \beta G_{13}^a \\
A_{12} & A_{22} & 0 & B_{12} & B_{22} & 0 & \beta C_{12} & \beta C_{22} & 0 & \beta G_{13}^a \\
0 & 0 & A_{66} & 0 & 0 & B_{66} & 0 & 0 & \beta C_{66} & 0 \\
B_{11} & B_{12} & 0 & D_{11} & D_{12} & 0 & \beta E_{11} & \beta E_{12} & 0 & \beta H_{13}^a \\
B_{12} & B_{22} & 0 & D_{12} & D_{22} & 0 & \beta E_{12} & \beta E_{22} & 0 & \beta H_{13}^a \\
0 & 0 & B_{66} & 0 & 0 & D_{66} & 0 & 0 & \beta E_{66} & 0 \\
C_{11} & C_{12} & 0 & E_{11} & E_{12} & 0 & \beta H_{11} & \beta H_{12} & 0 & \beta J_{13}^a \\
C_{12} & C_{22} & 0 & E_{12} & E_{22} & 0 & \beta H_{12} & \beta H_{22} & 0 & \beta J_{13}^a \\
0 & 0 & C_{66} & 0 & 0 & E_{66} & 0 & 0 & \beta H_{66} & 0 \\
\beta G_{13}^a & \beta G_{13}^a & 0 & \beta H_{13}^a & \beta H_{13}^a & 0 & \beta J_{13}^a & \beta J_{13}^a & 0 & \beta K_{13}^a
\end{bmatrix}\begin{Bmatrix}\varepsilon_{xx}^{(0)}\\\varepsilon_{yy}^{(0)}\\\gamma_{xy}^{(0)}\\\varepsilon_{xx}^{(1)}\\\varepsilon_{yy}^{(1)}\\\gamma_{xy}^{(1)}\\\varepsilon_{xx}^{(2)}\\\varepsilon_{yy}^{(2)}\\\gamma_{xy}^{(2)}\\\psi_z\end{Bmatrix} \tag{35}$$

$$[1-\mu\nabla^2]\begin{Bmatrix}R_{xz}\\R_{yz}\end{Bmatrix} = [1-\lambda\nabla^2]\begin{bmatrix}F_{55} & 0\\0 & F_{44}\end{bmatrix}\begin{Bmatrix}\gamma_{xz}^{(0)}\\\gamma_{yz}^{(0)}\end{Bmatrix} \tag{36}$$

where the stiffness coefficients are given as

$$\{A_{11},B_{11},C_{11},D_{11},E_{11},H_{11}\}=\int_{-h/2}^{h/2}\bar{Q}_{11}^{k}\left\{1,z,f(z),z^2,zf(z),\left(f(z)\right)^2\right\}\mathrm{d}z$$
$$\{A_{12},B_{12},C_{12},D_{12},E_{12},H_{12}\}=\int_{-h/2}^{h/2}\bar{Q}_{12}^{k}\left\{1,z,f(z),z^2,zf(z),\left(f(z)\right)^2\right\}\mathrm{d}z \tag{37}$$
$$\{A_{66},B_{66},C_{66},D_{66},E_{66},H_{66}\}=\int_{-h/2}^{h/2}\bar{Q}_{66}^{k}\left\{1,z,f(z),z^2,zf(z),\left(f(z)\right)^2\right\}\mathrm{d}z$$

$$F_{44}=F_{55}=\int_{-h/2}^{h/2}\bar{Q}_{44}^{k}\left(g(z)\right)^2\mathrm{d}z,\qquad K_{33}^{a}=\int_{-h/2}^{h/2}\bar{Q}_{33}^{k}\left(g'(z)\right)^2\mathrm{d}z,\{G_{13}^{a},H_{13}^{a},J_{13}^{a}\}=\int_{-h/2}^{h/2}\bar{Q}_{13}^{k}\{1,z,f(z)\}\mathrm{g}'(z)\mathrm{d}z$$

Therefore, the equation of motion of the nonlocal strain gradient nanoplate in terms of virtual displacements δu_0, δv_0, δw_0 and $\delta\varphi_z$ can be described by

$$(1-\lambda\nabla^2)\begin{bmatrix}A_{11}\dfrac{\partial^2u_0}{\partial x^2}+A_{66}\dfrac{\partial^2u_0}{\partial y^2}+(A_{12}+A_{66})\dfrac{\partial^2v_0}{\partial x\partial y}-B_{11}\dfrac{\partial^3w_0}{\partial x^3}-(B_{12}+2B_{66})\dfrac{\partial^3w_0}{\partial x\partial y^2}\\ -\beta\left(C_{66}\dfrac{\partial^5w_0}{\partial x^3\partial y^2}+(C_{12}+C_{66})\dfrac{\partial^5w_0}{\partial x\partial y^4}+C_{11}\dfrac{\partial^5w_0}{\partial x^5}\right)+G_{13}^{a}\dfrac{\partial\psi_z}{\partial x}\end{bmatrix}$$
$$=(1-\mu\nabla^2)\left[I_0\frac{\partial^2u_0}{\partial t^2}-I_1\frac{\partial^3w_0}{\partial x\partial t^2}-\beta J_1\frac{\partial^5w_0}{\partial x^3\partial t^2}\right] \tag{38}$$

$$(1-\lambda\nabla^2)\begin{bmatrix}A_{22}\dfrac{\partial^2v_0}{\partial y^2}+A_{66}\dfrac{\partial^2v_0}{\partial x^2}+(A_{12}+A_{66})\dfrac{\partial^2u_0}{\partial x\partial y}-B_{22}\dfrac{\partial^3w_0}{\partial y^3}-(B_{12}+2B_{66})\dfrac{\partial^3w_0}{\partial x^2\partial y}\\ -\beta\left(C_{66}\dfrac{\partial^5w_0}{\partial x^2\partial y^3}+(C_{12}+C_{66})\dfrac{\partial^5w_0}{\partial x^4\partial x}+C_{22}\dfrac{\partial^5w_0}{\partial y^5}\right)+G_{13}^{a}\dfrac{\partial\psi_z}{\partial y}\end{bmatrix}$$
$$=(1-\mu\nabla^2)\left[I_0\frac{\partial^2v_0}{\partial t^2}-I_1\frac{\partial^3w_0}{\partial y\partial t^2}-\beta J_1\frac{\partial^5w_0}{\partial y^3\partial t^2}\right] \tag{39}$$

$$(1-\lambda\nabla^2)\begin{bmatrix}B_{11}\dfrac{\partial^3u_0}{\partial x^3}+(B_{12}+2B_{66})\dfrac{\partial^3u_0}{\partial x\partial y^2}+(B_{12}+2B_{66})\dfrac{\partial^3v_0}{\partial x^2\partial y}+B_{22}\dfrac{\partial^3v_0}{\partial y^3}\\ -D_{11}\dfrac{\partial^4w_0}{\partial x^4}-2(D_{12}+2D_{66})\dfrac{\partial^4w_0}{\partial x^2\partial y^2}-D_{22}\dfrac{\partial^4w_0}{\partial y^4}+\beta\left[C_{11}\dfrac{\partial^5u_0}{\partial x^5}\right.\\ +(C_{12}+C_{66})\dfrac{\partial^5u_0}{\partial x\partial y^4}+(C_{12}+C_{66})\dfrac{\partial^5v_0}{\partial x^4\partial y}+C_{22}\dfrac{\partial^5v_0}{\partial y^5}+C_{66}\dfrac{\partial^5u_0}{\partial x^3\partial y^2}\\ +C_{66}\dfrac{\partial^5v_0}{\partial x^2\partial y^3}-2E_{11}\dfrac{\partial^6w_0}{\partial x^6}-2(E_{12}+2E_{66})\dfrac{\partial^6w_0}{\partial x^2\partial y^4}\\ \left.-2(E_{12}+2E_{66})\dfrac{\partial^6w_0}{\partial x^4\partial y^2}-2E_{22}\dfrac{\partial^6w_0}{\partial y^6}\right]-\beta^2\left[H_{11}\dfrac{\partial^8w_0}{\partial x^8}+2(H_{12}+H_{66})\dfrac{\partial^8w_0}{\partial x^4\partial y^4}\right.\\ +H_{66}\dfrac{\partial^8w_0}{\partial x^6\partial y^2}+H_{66}\dfrac{\partial^8w_0}{\partial x^2\partial y^6}+H_{22}\dfrac{\partial^8w_0}{\partial y^8}-F_{44}\dfrac{\partial^6w_0}{\partial x^6}-F_{55}\dfrac{\partial^6w_0}{\partial y^6}\Big]\\ +\beta J_{13}^{a}\left(\dfrac{\partial^4\psi_z}{\partial x^4}+\dfrac{\partial^4\psi_z}{\partial y^4}\right)+G_{13}^{a}\left(\dfrac{\partial^2\psi_z}{\partial x^2}+\dfrac{\partial^2\psi_z}{\partial y^2}\right)-F_{44}\dfrac{\partial^4\psi_z}{\partial y^4}-F_{55}\dfrac{\partial^4\psi_z}{\partial x^4}\end{bmatrix}$$
$$+(1-\mu\nabla^2)\left[q-f_e+\bar{N}_{xx}^{0}\frac{\partial^2w_0}{\partial x^2}+\bar{N}_{yy}^{0}\frac{\partial^2w_0}{\partial y^2}\right]$$
$$=(1-\mu\nabla^2)\left[I_0\frac{\partial^2w_0}{\partial t^2}+I_1\left(\frac{\partial^3u_0}{\partial x\partial t^2}+\frac{\partial^3v_0}{\partial y\partial t^2}\right)+\beta I_3\left(\frac{\partial^5u_0}{\partial x^3\partial t^2}+\frac{\partial^5v_0}{\partial y^3\partial t^2}\right)\right.$$
$$\left.-I_2\left(\frac{\partial^4w_0}{\partial x^2\partial t^2}+\frac{\partial^4w_0}{\partial y^2\partial t^2}\right)-2\beta I_4\left(\frac{\partial^6w_0}{\partial x^4\partial t^2}+\frac{\partial^6w_0}{\partial y^4\partial t^2}\right)-\beta^2I_5\left(\frac{\partial^8w_0}{\partial x^6\partial t^2}+\frac{\partial^8w_0}{\partial y^6\partial t^2}\right)+J_0\frac{\partial^2\psi_z}{\partial t^2}\right] \tag{40}$$

$$
\begin{aligned}
(1-\lambda\nabla^2)&\left[\begin{array}{c}-\beta G_{13}^{a}\left(\frac{\partial u_0}{\partial x}+\frac{\partial v_0}{\partial y}\right)+\beta H_{13}^{a}\left(\frac{\partial^2 w_0}{\partial x^2}+\frac{\partial^2 w_0}{\partial y^2}\right)+\beta^2(J_{13}^{a}-F_{55})\frac{\partial^4 w_0}{\partial x^4}\\ +\beta^2(J_{13}^{a}-F_{44})\frac{\partial^4 w_0}{\partial y^4}+\beta^2\left(F_{55}\frac{\partial^2\psi_z}{\partial x^2}+F_{44}\frac{\partial^2\psi_z}{\partial y^2}-K_{33}^{a}\psi_z\right)\end{array}\right]\\
&+(1-\mu\nabla^2)\left[\beta \mathrm{g}(z)\left(q-f_e+\bar{N}_{xx}^{0}\frac{\partial^2\ddot{\psi}_z}{\partial x^2}+\bar{N}_{yy}^{0}\frac{\partial^2\ddot{\psi}_z}{\partial y^2}\right)\right]\\
&=(1-\mu\nabla^2)\left[J_0\frac{\partial^2 w_0}{\partial t^2}+J_1\frac{\partial^2\psi_z}{\partial t^2}\right]
\end{aligned}
\tag{41}
$$

3. Analytical solution

In the present analysis, we develop a new analytical solution of Eqs. (38)-(41) using Galerkin method for nanoplates by considering different boundary conditions. The generalized displacements can be expressed as the following form:

$$
\begin{aligned}
u_0&=\sum_{m=1}^{\infty}\sum_{n=1}^{\infty}U_{mn}\frac{\partial X_m(x)}{\partial x}Y_n(y)e^{i\omega t},\\
v_0&=\sum_{m=1}^{\infty}\sum_{n=1}^{\infty}V_{mn}X_m(x)\frac{\partial Y_n(y)}{\partial y}e^{i\omega t}\\
\{w_0,\psi_z\}&=\sum_{m=1}^{\infty}\sum_{n=1}^{\infty}\{W_{mn},\Psi_{mn}\}X_m(x)Y_n(y)\,e^{i\omega t}
\end{aligned}
\tag{42}
$$

where, U_{mn}, V_{mn}, W_{mn} and Ψ_{mn} are arbitrary parameters. m and n are the mode shape numbers. $X_m(x)$ and $Y_n(y)$ are the functions that satisfy the boundary conditions. The boundary conditions of the laminated nanoplate in this analysis are fully simply supported (SSSS), fully clamped (CCCC), two opposite edges are simply supported and two other edges are clamped (CSCS), or two adjacent edges are clamped and two other edges are simply supported (CCSS). The functions $X_m(x)$ and $Y_n(y)$ that satisfy the proposed boundary conditions can be given as (Daikh *et al* 2021):

- $X_m(x)=\sin(\alpha x)$ and $Y_n(y)=\sin(\beta y)$, for the SSSS nanoplate.
- $X_m(x)=\sin^2(\alpha x)$ and $Y_n(y)=\sin^2(\beta y)$, for the CCCC nanoplate.
- $X_m(x)=\sin^2(\alpha x)$ and $Y_n(y)=\sin(\beta y)$, for the CCSS nanoplate.
- $X_m(x)=\sin(\alpha x)[\cos(\alpha x)-1]$ and $Y_n(y)=\sin(\beta y)[\cos(\beta y)-1]$, for the CSCS nanoplate.

where $\alpha=m\pi/a$, $\beta=n\pi/b$. By substituting Eqs. (42) in Eq. (38)-(41), one obtains

$$
([\mathrm{K}]_{4\times4}-\omega^2[M]_{4\times4})\begin{Bmatrix}U_{mn}\\V_{mn}\\W_{mn}\\\psi_z\end{Bmatrix}=\begin{Bmatrix}0\\0\\q\\0\end{Bmatrix}
\tag{43}
$$

where $[K]$ and $[M]$ are the rigidity and mass matrices, respectively.

$$
q=q_0\int_0^a\int_0^b\sin(\alpha x)\sin(\alpha x)\sin(\beta y)\sin(\beta y)\,\mathrm{d}x\mathrm{d}y
\tag{44}
$$

For the bending analysis, the sinusoidal applied load is given as (Thai *et al*. 2014):

4. Results and discussions

The analyzed nanoplate is made of a mixture of the polymer PmPV as matrix and armchair (10, 10) single walled CNTs as reinforcement. The nanoplate is exposed to in-plane load in two directions $\left(\bar{N}_{xx}^{0}=\chi_1 N_{cr},\ \bar{N}_{yy}^{0}=\chi_2 N_{cr}\right)$ for buckling analysis and transverse sinusoidal loading for the bending analysis. Material properties of the CNTs are stated in Table 1, while the temperature dependent material properties of the polymer PmPV are given as (Shen 2009),

$$
\begin{aligned}
E_m&=(3.51-0.0047\Delta T)\ \mathrm{GPa},\\
\alpha_m&=45(1+0.0005\Delta T)10^{-6}\quad 1/°K
\end{aligned}
\tag{45}
$$

Poisson ratio and the mass density are given as $v_m=0.34$ and $\rho_m=1150\mathrm{kg/m^3}$, respectively. Since this study aims to carry out the effect of thermal environment on the response of CNTRC laminated nanoplates, it is necessary to obtain the material properties of CNTs as a function of temperature, hence, Daikh *et al* (2020a) proposed a formulation of CNTs material properties based on Touloukian principal (Touloukian 1967), which can be written as

$$
P=P_0(P_{-1}T^{-1}+1+P_1T+P_2T^2+P_3T^3)
\tag{46}
$$

where $T=T_0+\Delta T$. T_0 is the ambient $(T_0=300\,°K)$, and ΔT is the temperature difference, and P_0, P_1, P_2, and P_3 are coefficients of temperature (see Table 2).

To standardize and simplify calculations, the normalized parameters for bending, buckling and vibration analyses of CNTRC laminated nanoplates are described using the following forms:

The dimensionless displacements:

$$
\bar{w}=\frac{10^3 D_0}{a^4 q_0}w\left(\frac{a}{2},\frac{b}{2}\right)\quad,\quad \&\ D_0=\frac{E_p^0 h^3}{12\left(1-\upsilon_p{}^2\right)}
\tag{47}
$$

where E_p^0 is the polymer PmPV Young's modulus at the ambient temperature $(T_0=300\,°K)$. The dimensionless critical buckling loads, the dimensionless frequency, and the foundation parameters:

Table 1 Thermomechanical properties of (10, 10) SWCNT

$T[K]$	E_{11}^{cnt}[TPa]	E_{22}^{cnt}[TPa]	G_{12}^{cnt}[TPa]	ν_{11}^{cnt}	$\alpha_{11}^{cnt}[10^{-6}/°K]$	$\alpha_{22}^{cnt}[10^{-6}/°K]$
300	5.6466	7.0800	1.9445	0.175	3.4584	5.1682
400	5.5679	6.9814	1.9703	0.175	4.1496	5.0905
500	5.5308	6.9348	1.9643	0.175	4.5361	5.0189
700	5.4744	6.8641	1.9644	0.175	4.6677	4.8943

Table 2 Temperature-dependent coefficients of CNTs material properties

	P_0	P_{-1}	P_1	P_2	P_3
E_{11}^{cnt}[TPa]	6.3998	0	-6.77898×1e-4	1.16097×1e-6	-6.96636×1e-10
E_{22}^{cnt}[TPa]	8.02155	0	-6.75726×1e-4	1.15626×1e-6	-6.93444×1e-10
G_{12}^{cnt}[TPa]	1.40755	0	2.46968×1e-3	-4.94831×1e-6	3.18224×1e-9
$\alpha_{11}[10^{-6}/°K]$	-1.12515	0	-2.03678×1e-2	2.56588×1e-5	-1.00986×1e-8
$\alpha_{22}[10^{-6}/°K]$	5.43715	0	-1.81092×1e-4	5.33367×1e-8	2.29899×1e-12

$$\bar{N} = N_{cr}\frac{a^2}{D_0\pi^2}, \quad \bar{\omega} = \omega h\sqrt{\frac{\rho_p}{E_p^0}}, \qquad k_w = \frac{a^2b^2}{D_0}K_w \tag{48}$$

To standardize and simplify calculations, the normalized parameters for bending, buckling and vibration analyses of CNTRC laminated nanoplates are described using the following forms:

$$\bar{w} = \frac{10^3 D_0}{a^4 q_0} w\left(\frac{a}{2}, \frac{b}{2}\right), \quad \& D_0 = \frac{E_p^0 h^3}{12\left(1-{\upsilon_p}^2\right)} \tag{47}$$

The dimensionless displacements:

$$q\bar{N} = N_{cr}\frac{a^2}{D_0\pi^2}, \quad \bar{\omega} = \omega h\sqrt{\frac{\rho_p}{E_p^0}}, \qquad k_w = \frac{a^2b^2}{D_0}K_w \tag{48}$$

where E_p^0 is the polymer PmPV Young's modulus at the ambient temperature $(T_0 = 300\,°K)$. The dimensionless critical buckling loads, the dimensionless frequency, and the foundation parameters:

4.1 Verification analysis

The results for deflections and stresses of simply supported cross-ply laminated composite plate are compared with those generated in literature using analytical solutions based on Navier's technique (Table 3). The used material properties are: $E_1 = 25E_2$; $G_{12} = G_{13} = 0.5E_2$; $G_{23} = 0.2E_2$; $\nu_{12} = 0.25$. All results are compared with the analytical solution of Reddy (Reddy 1984). Of all the theories used, it can be observed that the results computed by the proposed theory are absolutely identical with those obtained by Reddy using the TSDT.

To confirm the efficacy of the proposed theory, Table 4 is carried out to compare our results with the analytical solution of Wattanasakulpong and Chaikittiratana (2015) using TSDT and SSDT with and without considering the thickness stretching effect. It can be observed that the inclusion of the thickness stretching effect has a remarkable impact on the results. In addition, it is clear that the proposed solutions are in good agreement with the results obtained by the other theories.

4.2 Parametric study

4.2.1 Bending analysis

In order to examine the response of CNTRC laminated plates subjected to transverse sinusoidal loadings, Table 5 represents dimensionless central deflection by considering the impact of CNTs volume fraction, CNTs distribution patterns, power-law index and number of layers *N*. It can be observed that the mentioned parameters have a significant effect on the bending response.

In Table 6, the impact of geometric parameters a, b, and h on the central deflection of the composite laminated plates is illustrated for various multilayered schemes. It is noticed that the transverse displacement decreases by increasing of thickness parameter *a/h* and is directly proportional of aspect ratio *b/a*. In Table 7, we presented the impact of various boundary conditions, thermal environment, nonlocal and length scale parameters on the displacement of FG-X CNTRC laminated nanoplates (0°/90°). The effect of the proposed various two-dimensional Winkler elastic foundation on deflection of simply supported FG-X CNTRC laminated plate (0°/90°) is investigated in Table 8. It can be observed that the increase of the parameters κ and ξ leads to a decrement of central deflection, which are more influenced by the first factor κ. In the present study, we proposed a formulation of the volume fraction CNTs based on power-law function, therefore, in Fig. 5, we investigated the effect of power-law index k on the dimensionless central deflection of single layer CNTRC plate using various CNTs distribution patterns. The value of the index k ranges from 0.2 to 5. It is obvious from the figure that the index k has a significant impact on the bending plate response, where the increase of index k leads to sharp decrement of central deflection for the FG-O CNTRC plates, and causes a little and large increment of central deflection for the FG-X and FG-V CNTRC plates, respectively. In Fig. 6, the influence of the volume fraction of CNTs in the FG-X composite plate is investigated. It can be observed that the central deflection decreases by the increase of CNTs volume fraction, (i.e., increase of the plate stiffness).

Table 3 Nondimensional* deflection and stresses in [0°/90°/90°/0°] square laminated composite plate (a/h = 4)

Source	$\widetilde{w}$	Diff.%	$\tilde{\sigma}_{xx}$	Diff.%	$\tilde{\sigma}_{yy}$	Diff.%	$\tilde{\tau}_{yz}$	Diff.%	$\tilde{\tau}_{xy}$	Diff.%	$\tilde{\tau}_{xz}$	Diff.%	Avg.%
Reddy (1984)	1.8937	-	0.6651	-	0.6322	-	0.2389	-	0.0440	-	0.2064	-	
Touratier (1991)	1.9088	0,80	0.6830	2,69	0.6349	0,43	0.2462	3,06	0.0450	2,27	0.2162	4,75	2,33
Soldatos (1992)	1.8920	-0,09	0.6601	-0,75	0.6302	-0,32	0.2804	17,37	0.0438	-0,45	0.2272	10,08	4,84
Nguyen (2013)	1.9218	1,48	0.7232	8,74	0.6341	0,30	0.2768	15,86	0.0469	6,59	0.2174	5,33	6,38
Thai (2014)	1.9258	1,70	0.7121	7,07	0.6366	0,70	0.2768	15,86	0.0466	5,91	0.2183	5,77	6,17
Singh (2017)	1.9213	1,46	0.6936	4,29	0.6482	2,53	0.2650	10,93	0.0473	7,50	0.2218	7,46	5,69
Present $(\varepsilon = 0)$	1.8935	-0,01	0.6643	-0,12	0.6322	0,00	0.2389	0,00	0.0440	0,00	0.2063	-0,05	0,03

*$\widetilde{w} = 10^2 \left(\frac{h^3 E_2}{q_0 a^4}\right) w\left(\frac{a}{2},\frac{b}{2}\right)$,$\tilde{\sigma}_{xx} = -\frac{h^2}{a^2 q_0}\sigma_{xx}\left(\frac{a}{2},\frac{b}{2},\frac{h}{2}\right)$,$\tilde{\sigma}_{yy} = -\frac{h^2}{a^2 q_0}\sigma_{yy}\left(\frac{a}{2},\frac{b}{2},\frac{h}{4}\right)$, $\tilde{\tau}_{yz} = \frac{h}{a q_0}\tau_{yz}\left(\frac{a}{2},0,0\right)$,$\tilde{\tau}_{xz} = \frac{h}{a q_0}\tau_{xz}\left(0,\frac{b}{2},0\right)$, $\tilde{\tau}_{xy} = \frac{h^2}{a^2 q_0}\tau_{xy}\left(0,0,-\frac{h}{2}\right)$.

Table 4 Dimensionless central deflection of simply supported single layer CNTRC square plates (a/h = 10)

	$V^*_{CNT} = 0.11$				$V^*_{CNT} = 0.14$				$V^*_{CNT} = 0.17$			
	UD	FG–X	FG–O	FG–V	UD	FG–X	FG–O	FG–V	UD	FG–X	FG–O	FG–V
TSDT(*) $\varepsilon = 0$	0.4964	0.4227	0.7081	0.5869	0.4396	0.3817	0.6148	0.5133	0.3177	0.2723	0.4526	0.3769
TSDT $\varepsilon \neq 0$	0.4983	0.4238	0.7129	0.5893	0.4408	0.3825	0.6181	0.5149	0.3188	0.2731	0.4552	0.3781
SSDT(*) $\varepsilon = 0$	0.4953	0.4208	0.7104	0.5859	0.4383	0.3800	0.6168	0.5121	0.3170	0.2715	0.4537	0.3763
SSDT $\varepsilon \neq 0$	0.4971	0.4219	0.7149	0.5881	0.4395	0.3807	0.6198	0.5137	0.3181	0.2722	0.4560	0.3774
Present $\varepsilon = 0$	0.4964	0.4229	0.7081	0.5871	0.4397	0.3819	0.6149	0.5134	0.3177	0.2725	0.4526	0.3770
Present $\varepsilon \neq 0$	0.4985	0.4240	0.7130	0.5895	0.4410	0.3827	0.6181	0.5151	0.3189	0.2732	0.4553	0.3782

(*) Results obtained by Wattanasakulpong and Chaikittiratana (2015)

Table 5 Effect of number of bi-layers and power-law index of the CNTs distributions on dimensionless deflection of simply supported CNTRC laminated plate $(a = b, a/h = 10, T_0 = 300\,°K)$

Config.	k	$V^*_{cnt} = 0.11$			$V^*_{cnt} = 0.14$			$V^*_{cnt} = 0.17$		
		FG–X	FG–O	FG–V	FG–X	FG–O	FG–V	FG–X	FG–O	FG–V
$(0°/90°)_1$	0.5	0.5919	1.5963	0.7812	0.4939	1.4240	0.6569	0.3755	1.0403	0.4961
	1	0.6530	1.2331	1.0363	0.5477	1.0674	0.8896	0.4180	0.7907	0.6657
	2	0.7600	0.9479	1.4276	0.6419	0.8030	1.2790	0.4900	0.6002	0.9216
	5	1.0103	0.7161	1.7970	0.8677	0.5974	1.7078	0.6466	0.4488	1.1032
$(0°/90°)_3$	0.5	0.3376	0.5350	0.3419	0.2884	0.4555	0.2922	0.2134	0.3482	0.2162
	1	0.4011	0.4130	0.4096	0.3421	0.3525	0.3495	0.2572	0.2648	0.2627
	2	0.5146	0.3444	0.5302	0.4373	0.2941	0.4510	0.3339	0.2173	0.3442
	5	0.7915	0.2989	0.8193	0.6735	0.2549	0.6992	0.5166	0.1855	0.5341
$(0°/90°)_5$	0.5	0.3275	0.5101	0.3289	0.2800	0.4342	0.2813	0.2069	0.3319	0.2079
	1	0.3902	0.3942	0.3930	0.3331	0.3366	0.3356	0.2501	0.2527	0.2520
	2	0.5026	0.3296	0.5079	0.4275	0.2816	0.4321	0.3263	0.2079	0.3298
	5	0.7789	0.2871	0.7883	0.6627	0.2450	0.6714	0.5090	0.1781	0.5150

One of the objectives of this work is to improve the mechanical behaviour of composite plates. The use of cross-ply multilayers can increase the plate stiffness. From Fig.7, it is seen that the central deflections decrease by the increasing of the number of bi-layers (increasing the plate stiffness), for various CNTRC patterns. When $N \geq 4$, the central deflection remains constant. Fig. 8 shows the effect of aspect ratio *b/a* and thickness ratio *a/h* on dimensionless central deflection of simply supported CNTRC laminated plate [0°/90°/0°/90°]. It is noticed that the central deflections are directly and inversely proportional to *b/a* and *a/h*, respectively.

Table 6 Effect of the geometric parameters and the number of layers on the central deflection of simply supported FG CNTRC laminated plate $(V_{cnt}^{*} = 0.11, k = 1, T_0 = 300\ °K)$

Config.	*b/a*	*a/h*				
		5	10	20	50	100
$(0°/90°)_1$	0.5	0.2416	0.1143	0.0784	0.0679	0.0664
	1	0.9876	0.6530	0.5670	0.5427	0.5392
	2	1.8284	1.2537	1.1045	1.0622	1.0561
	3	1.9850	1.3473	1.1832	1.1369	1.1303
$(0°/90°)_3$	0.5	0.2440	0.0912	0.0468	0.0335	0.0316
	1	0.8181	0.4011	0.2932	0.2627	0.2584
	2	1.4590	0.7483	0.5595	0.5055	0.4978
	5	1.6039	0.8050	0.5962	0.5370	0.5285
$(0°/90°)_5$	0.5	0.2419	0.0896	0.0454	0.0323	0.0303
	1	0.8055	0.3902	0.2827	0.2524	0.2481
	2	1.4342	0.7270	0.5391	0.4853	0.4776
	3	1.5776	0.7822	0.5743	0.5154	0.5069

Table 7 Effect of temperature, nonlocal and length scale parameters on dimensionless central deflection of the CNTRC laminated nanoplate $(V_{cnt}^{*} = 0.11,\ a = b,\ a/h = 10,\ k = 1)$

BCs.	μ	λ	Temperature ($°K$)				
			300	400	500	600	700
SSSS	0	0	0.4240	0.5056	0.6473	0.9690	2.4779
		1	0.3541	0.4222	0.5406	0.8093	2.0694
		2	0.3040	0.3625	0.4641	0.6948	1.7765
	1	0	0.5077	0.6054	0.7751	1.1603	2.9670
		1	0.4240	0.5056	0.6473	0.9690	2.4779
		2	0.3640	0.4340	0.5557	0.8319	2.1272
	2	0	0.5914	0.7052	0.9028	1.3516	3.4561
		1	0.4939	0.5889	0.7540	1.1288	2.8863
		2	0.4240	0.5056	0.6473	0.9690	2.4779
CCCC	0	0	0.3711	0.4600	0.6129	0.9416	2.1729
		1	0.2425	0.3006	0.4006	0.6156	1.4215
		2	0.1800	0.2232	0.2975	0.4573	1.0562
	1	0	0.4444	0.5508	0.7339	1.1274	2.6018
		1	0.2903	0.3600	0.4797	0.7372	1.7021
		2	0.2156	0.2673	0.3563	0.5476	1.2647
	2	0	0.5177	0.6417	0.8549	1.3133	3.0307
		1	0.3382	0.4193	0.5588	0.8587	1.9827
		2	0.2511	0.3114	0.4150	0.6379	1.4731

Table 8 Effect of Winkler elastic foundation parameters on bending deflection of simply supported FG-X CNTRC laminated plate (0°/90°) $(V_{cnt}^{*} = 0.11,\ a = b, a/b = 10,\ k = 1, T_0 = 300\ °K)$

κ	ξ	Sinusoidal	Reverse sinusoidal	Parabolic	Reverse parabolic
10	10	0.6446	0.6488	0.6485	0.6449
	10^2	0.6094	0.6488	0.6462	0.6118
	10^3	0.3942	0.6488	0.6236	0.4041
10	10	0.6094	0.6132	0.6129	0.6097
	10^2	0.5779	0.6132	0.6108	0.5800

Table 8 Continued

κ	ξ	Sinusoidal	Reverse sinusoidal	Parabolic	Reverse parabolic
10	10^3	0.3808	0.6132	0.5906	0.3900
	10	0.3942	0.3958	0.3957	0.3943
10^3	10^2	0.3808	0.3958	0.3948	0.3817
	10^3	0.2839	0.3958	0.3863	0.2890

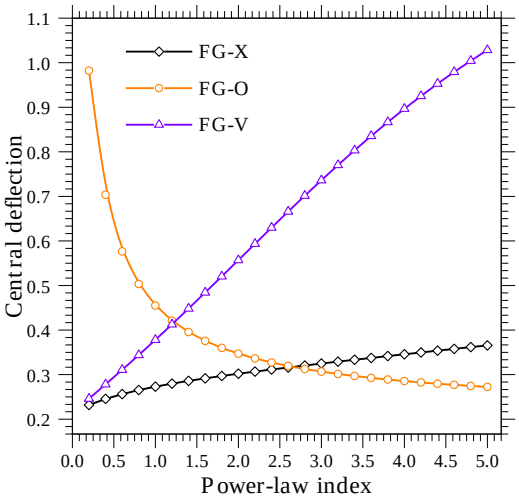

Fig. 5 Effect of power-law index on dimensionless central deflection of simply supported square single layer CNTRC plate $(V^*_{cnt} = 0.11, a/h = 10)$

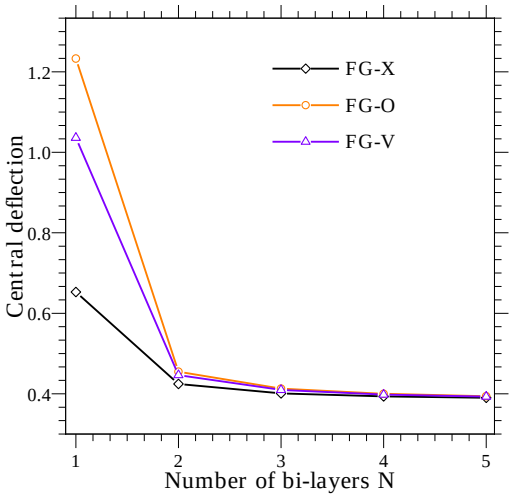

Fig. 7 Effect of number of layers N on dimensionless central deflection of simply supported square CNTRC laminated plate $(V^*_{cnt} = 0.11, a/h = 10, k = 1)$

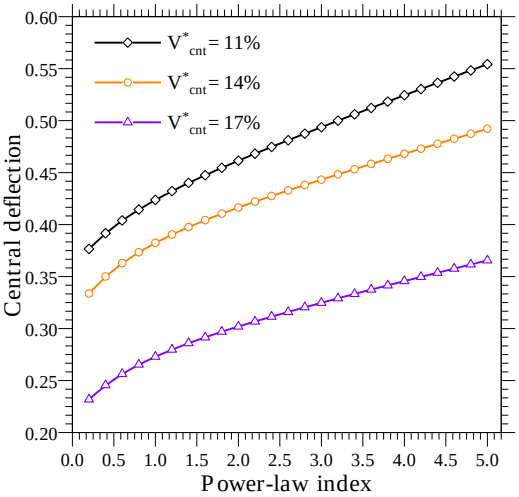

Fig. 6 Effect of power-law index on dimensionless central deflection of simply supported single layer FG-X CNTRC plate $(b/a = 1, a/h = 10)$

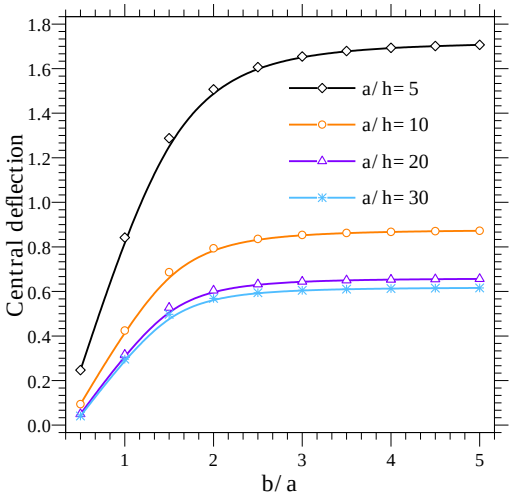

Fig. 8 Effect of aspect ratio *b/a* and thickness ratio *a/h* on dimensionless central deflection of simply supported CNTRC laminated plate [0°/90°/0°/90°] $(V^*_{cnt} = 0.11, k = 1)$

The influence of high thermal environment on bending response of various CNTRC multilayers is presented in Fig. 9. The results show that the high temperature decreases the plate stiffness, therefore increases the plate deflection. It can be concluded from this figure the single layer CNTRC plate is more influenced by the temperature than mult-ilayered plates. The impact of various Winkler elastic foundations on the transverse displacement of the CNTRC plate in the *x*-direction is investigated in Fig. 10. It can be observed that plates resting on the sinusoidal and the reverse parabolic foundations have the less deflections than the other foundations.

Moreover, in Fig. 11, the effect of the parameters of the elastic foundation κ and ξ on dimensionless central deflection of square FG-X CNTRC laminated nanoplate is presented. It can be seen that the deflection $\bar{w}$ decreases by increasing of the elastic foundation parameters. The effect of nonlocal and length scale parameters on dimensionless central deflection of square [0°/90°] CNTRC laminated

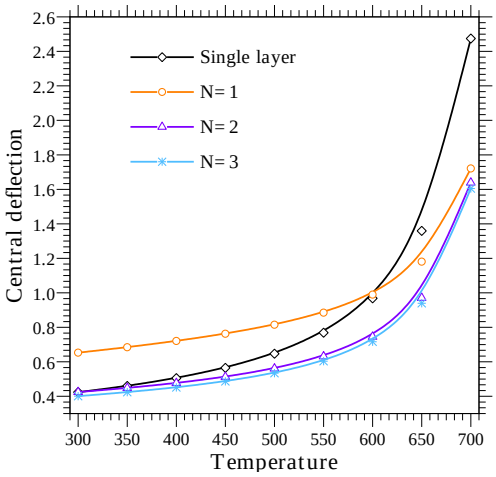

Fig. 9 Effect of temperature on dimensionless central deflection of simply supported square CNTRC laminated plate $(V_{cnt}^{*} = 0.11, a/h = 10, k = 1)$

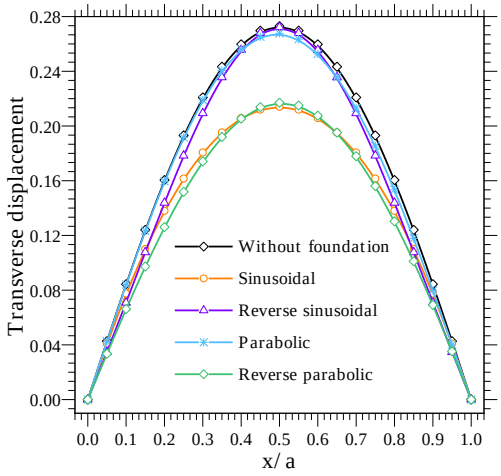

Fig. 10 Effect of various Winkler elastic foundation on dimensionless central deflection of simply supported square CNTRC plate $(V_{cnt}^{*} = 0.11, a/h = 10, k = 1)$

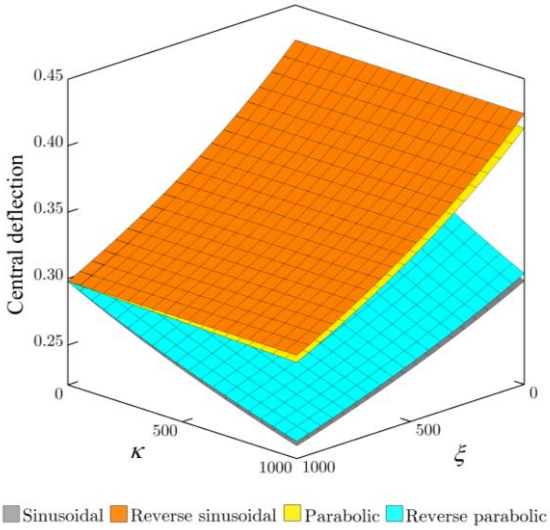

Fig. 11 Effect of elastic foundation parameters on dimensionless central deflection of square simply supported FG-X CNTRC plate $(V_{cnt}^{*} = 0.11, a/h = 10, k = 1)$

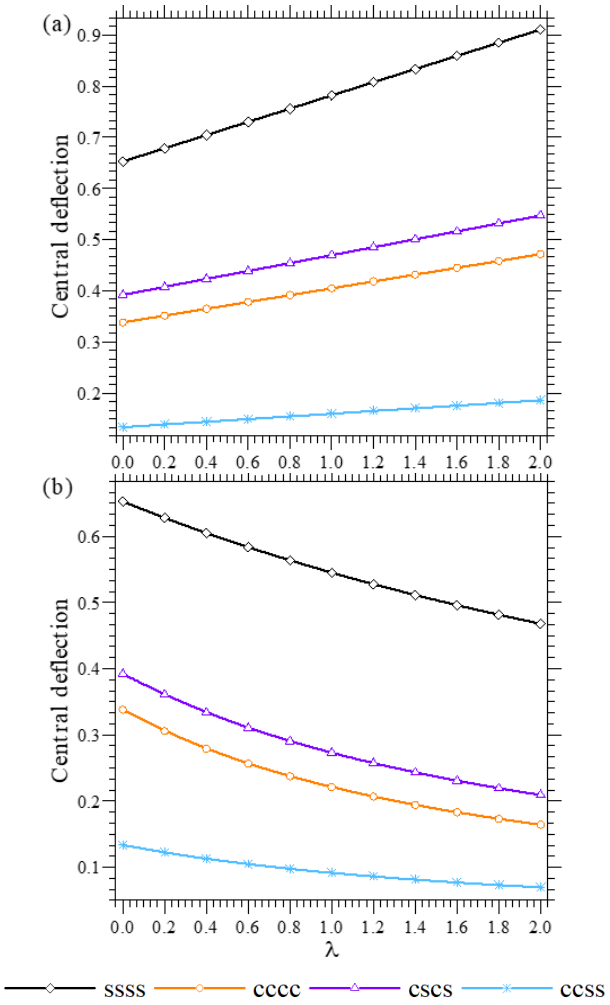

Fig. 12 Effect of nonlocal parameter and length scale parameter on dimensionless central deflection of square FG-X CNTRC laminated nanoplate [0°/90°] $(V_{cnt}^{*} = 0.11, a/h = 10, k = 1)$

nanoplate is presented in Fig. 12 for various boundary conditions. It can be observed that the augment of the nonlocal parameter μ reduces the CNTRC laminated nanoplate stiffness and therefore leads to augmentation in central deflection. Furthermore, unlike the effect of nonlocality, the central deflection decreases by increasing length-scale parameter λ. It seems that the nonlocal parameter has more influence in comparison with length scale parameter.

4.2.2 Buckling analysis

Table 9 presents dimensionless critical buckling load of multilayered CNTRC plate subjected to uniaxial or biaxial compressive loadings. The influences of CNTs volume fraction, CNTs distribution patterns, power-law index and number of bi-layers N are investigated. In Table 10, the response of bilayer FG-X CNTRC laminated nanoplates (0°/90°) subjected to biaxial compressive loads is examined by considering the temperature effect, nonlocal and length scale parameters effect. it can be seen that the inclusion of temperature and nonlocal parameter μ reduces the critical buckling load contradicting the length scale parameter λ.

Table 9 Effect of number of bilayer, power-law index and the CNTs distributions on dimensionless frequencies of simply supported CNTRC plates $(a = b, a/h = 10, T = 300°\text{K})$

Config.	k	$V^*_{cnt} = 0.11$			$V^*_{cnt} = 0.14$			$V^*_{cnt} = 0.17$		
		FG–X	FG–O	FG–V	FG–X	FG–O	FG–V	FG–X	FG–O	FG–V
Uniaxial compressive load										
$(0°/90°)_1$	0.5	17.4182	6.4755	13.2078	20.8627	7.2573	15.6994	27.4524	9.9357	20.7943
	1	15.7941	8.3777	9.9651	18.8211	9.6749	11.6039	24.6674	13.0630	15.5098
	2	13.5812	10.8914	7.2438	16.0703	12.8512	8.0826	21.0655	17.1973	11.2248
	5	10.2349	14.4063	5.7661	11.9113	17.2600	6.0663	16.0059	22.9793	9.4102
$(0°/90°)_2$	0.5	28.6005	17.4285	27.7469	33.5391	20.4460	32.5191	45.2245	26.7731	43.8619
	1	24.2377	22.6146	23.0465	28.4603	26.5023	27.0324	37.8063	35.2546	35.9224
	2	19.0908	27.2489	17.7552	22.4746	31.9387	20.8488	29.4392	43.1477	27.3603
	5	12.6399	31.6285	11.6366	14.8346	37.1439	13.5557	19.4324	50.9056	17.9584
$(0°/90°)_3$	0.5	30.4300	19.2533	30.0485	35.5960	22.5947	35.1391	48.1457	29.5826	47.5367
	1	25.6402	24.9075	25.1128	30.0418	29.1553	29.4091	39.9962	38.8444	39.1620
	2	20.0226	29.8364	19.4355	23.5401	34.9073	22.8265	30.8581	47.2809	29.9442
	5	13.0561	34.3435	12.6152	15.3318	40.2456	14.7715	20.0249	55.3424	19.3769
Biaxial compressive load										
$(0°/90°)_1$	0.5	8.7091	3.2377	6.6039	10.4313	3.6287	7.8497	13.7262	4.9678	10.3971
	1	7.8970	4.1889	4.9826	9.4106	4.8374	5.8020	12.3337	6.5315	7.7549
	2	6.7906	5.4457	3.6219	8.0351	6.4256	4.0413	10.5327	8.5987	5.6124
	5	5.1174	7.2032	2.8830	5.9557	8.6300	3.0332	8.0029	11.4896	4.7051
$(0°/90°)_2$	0.5	14.3002	8.7142	13.8735	16.7695	10.2230	16.2596	22.6123	13.3865	21.9309
	1	12.1189	11.3073	11.5233	14.2302	13.2511	13.5162	18.9032	17.6273	17.9612
	2	9.5454	13.6245	8.8776	11.2373	15.9693	10.4244	14.7196	21.5739	13.6801
	5	6.3199	15.8142	5.8183	7.4173	18.5720	6.7778	9.7162	25.4528	8.9792
$(0°/90°)_3$	0.5	15.2150	9.6266	15.0242	17.7980	11.2974	17.5696	24.0729	14.7913	23.7683
	1	12.8201	12.4538	12.5564	15.0209	14.5777	14.7046	19.9981	19.4222	19.5810
	2	10.0113	14.9182	9.7177	11.7701	17.4536	11.4133	15.4291	23.6405	14.9721
	5	6.5281	17.1718	6.3076	7.6659	20.1228	7.3857	10.0124	27.6712	9.6884

Table 10 Effect of temperature, nonlocal and length scale parameters on dimensionless critical buckling load $(V^*_{cnt} = 0.11, a = b, a/h = 10, k = 1)$

μ	λ	Temperature °K				
		300	400	500	600	700
0	0	7.8970	7.1495	6.3154	5.1925	2.9697
	1	9.4558	8.5607	7.5620	6.2175	3.5559
	2	11.0147	9.9720	8.8086	7.2424	4.1421
1	0	6.5952	5.9709	5.2743	4.3365	2.4802
	1	7.8970	7.1495	6.3154	5.1925	2.9697
	2	9.1989	8.3281	7.3564	6.0485	3.4593
2	0	5.6618	5.1259	4.5278	3.7228	2.1292
	1	6.7794	6.1377	5.4216	4.4577	2.5494
	2	7.8970	7.1495	6.3154	5.1925	2.9697

The influence played by power-law index on the buckling response of single layer CNTRC plate is displayed in Fig. 13 using various CNTs distribution patterns. It is seen that the increase of index k leads to increment of dimensionless critical buckling load for the FG-O CNTRC plates unlike the FG-X and FG-V CNTRC plates.

Effect of number of layers N on dimensionless critical buckling load of square CNTRC laminated plate is plotted in Fig. 14. The use of more than four layers can improve the plate stiffness and can offer excellent results. Fig. 15

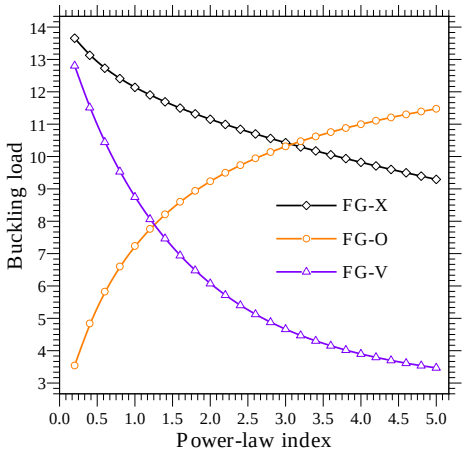

Fig. 13 Effect of power-law index on dimensionless critical buckling load of simply supported square single layer CNTRC plate $(V_{cnt}^{*} = 0.11, a/h = 10)$

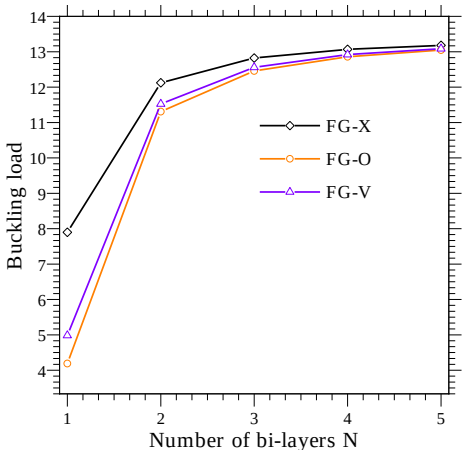

Fig. 14 Effect of number of layers N on dimensionless critical buckling load of simply supported square CNTRC plate $(V_{cnt}^{*} = 0.11, a/h = 10, k = 1)$

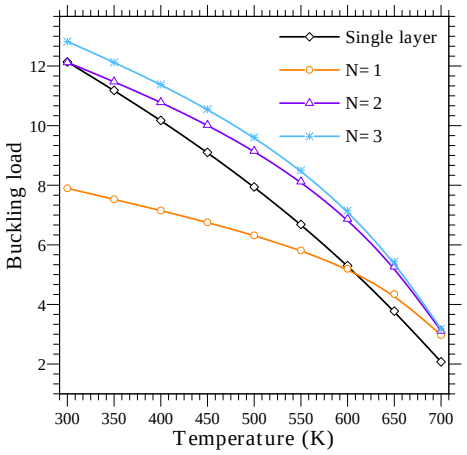

Fig. 15 Effect of temperature on dimensionless critical buckling load of simply supported square CNTRC plate $Vcnt*$=0.11, a/h=10, k=1

exhibits the effect of temperature and number of layers on dimensionless critical buckling load of square CNTRC laminated plate. It is clear that the existence of high temperature significantly reduces the buckling capacity of

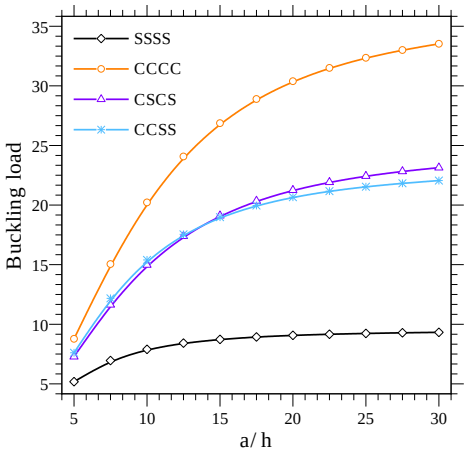

Fig. 16 Effect of thickness ratio *a/h* on dimensionless critical buckling load of FG-X CNTRC plate $(V_{cnt}^{*} = 0.11, b/a = 1, k = 1)$

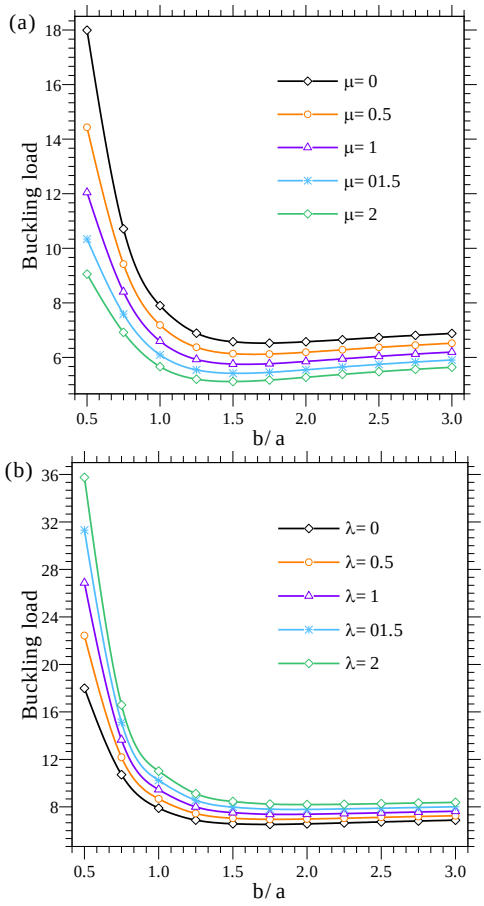

Fig. 17 Effect of aspect ratio *b/a* nonlocal parameter μ on dimensionless critical buckling load of simply supported [0°/90°] FG-X CNTRC plate $(V_{cnt}^{*} = 0.11, a/h = 10, k = 1)$

CNTRC plates, whereas the number of bilayers improves it. Effect of thickness ratio *a/h* on dimensionless critical buckling load of FG-X CNTRC plate under various boundary conditions is showed in Fig. 16. The highest values of critical buckling load are occurred for the fully clamped plate (CCCC), while the lowest values are for the simply supported plate. Effects of plate aspect ratio *b/a*,

Table 11 Effect of modes and power-law index on dimensionless frequencies of simply supported FG-X CNTRC laminated plate $\left(V_{cnt}^{*}=0.11, a=b, \frac{a}{h}=10,\ T=300°\text{K}\right)$

Config.	mode	k				
		0.5	1	2	3	5
$(0°/90°)_1$	(1, 1)	0.1226	0.1171	0.1090	0.1031	0.0949
	(1, 2)	0.2854	0.2749	0.2596	0.2483	0.2320
	(2, 2)	0.3808	0.3675	0.3482	0.3340	0.3138
	(1, 3)	0.4826	0.4675	0.4469	0.4322	0.4110
	(2, 3)	0.5375	0.5208	0.4977	0.4813	0.4578
$(0°/90°)_3$	(1, 1)	0.1627	0.1499	0.1329	0.1217	0.1076
	(1, 2)	0.3240	0.3080	0.2858	0.2700	0.2479
	(2, 2)	0.4218	0.4032	0.3773	0.3589	0.3329
	(1, 3)	0.4965	0.4790	0.4559	0.4395	0.4159
	(2, 3)	0.5566	0.5371	0.5111	0.4929	0.4669
$(0°/90°)_5$	(1, 1)	0.1652	0.1520	0.1345	0.1230	0.1085
	(1, 2)	0.3273	0.3106	0.2877	0.2715	0.2490
	(2, 2)	0.4257	0.4062	0.3795	0.3605	0.3341
	(1, 3)	0.5005	0.4816	0.4570	0.4401	0.4159
	(2, 3)	0.5610	0.5400	0.5126	0.4937	0.4673

Table 12 Effect of temperature, nonlocal and length scale parameters on dimensionless frequency $(V_{cnt}^{*}=0.11, a=b, a/h=10, k=1)$

μ	λ	Temperature				
		300	400	500	600	700
0	0	0.1171	0.1115	0.1049	0.0952	0.0721
	1	0.1282	0.1220	0.1147	0.1042	0.0789
	2	0.1383	0.1317	0.1238	0.1124	0.0851
1	0	0.1070	0.1019	0.0958	0.0870	0.0659
	1	0.1171	0.1115	0.1049	0.0952	0.0721
	2	0.1264	0.1203	0.1132	0.1027	0.0778
2	0	0.0992	0.0944	0.0888	0.0806	0.0610
	1	0.1085	0.1033	0.0972	0.0882	0.0668
	2	0.1171	0.1115	0.1049	0.0952	0.0721

nonlocal and length scale parameters on dimensionless critical buckling load of square [0°/90°] CNTRC laminated nanoplates are presented in Fig. 17. It is seen that the increase of the nonlocal parameter μ reduce the CNTRC plate stiffness and therefore lead to a reduction in critical buckling loads, while the results of critical buckling loads increase by increasing of length-scale parameter λ. As in the previous analysis, the nonlocal parameter has more influence in comparison with length scale parameter.

4.2.3 Free vibration analysis

The influence of the number of layers *N* and power-law index on dimensionless frequencies simply supported FG-X CNTRC plate is presented in Table 11 considering various mode shapes.

The increase of the number of layers *N* leads to a slight increment of dimensionless frequencies, unlike the power-law index. Table 12 presents the effect of applied temperature, nonlocal and length scale parameters on free vibration response of CNTRC laminated nanoplates (0°/90°). It is clear that the natural frequencies increase by increasing of length scale parameter and by decreasing of temperature and nonlocal parameter.

The influence played by power-law index on the dimensionless natural frequencies of single layer CNTRC plate is examined in Fig. 18 for various CNTs distribution patterns. It is observed from this figure, the increase of index k leads to increment of dimensionless natural frequencies for the FG-O CNTRC plates, unlike the FG-X and FG-V CNTRC plates. Fig. 19 depicts the temperature effect on the CNTRC plate (0°/90°) with various distribution patterns of CNTs. It is observed that the increase of temperature reduces the plate stiffness, therefore the natural frequencies. The influence of nonlocal parameter

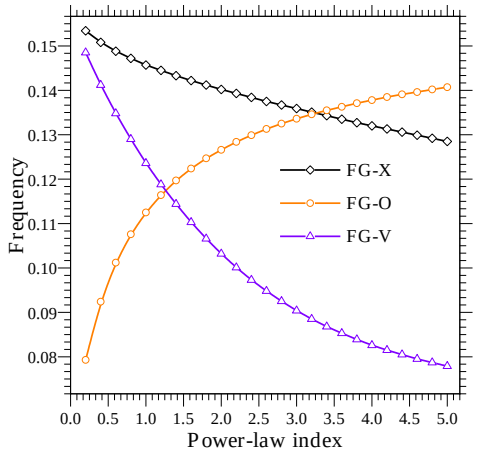

Fig. 18 Effect of power-law index on dimensionless frequency of simply supported square single layer CNTRC plate $(V_{cnt}^{*} = 0.11, a/h = 10)$

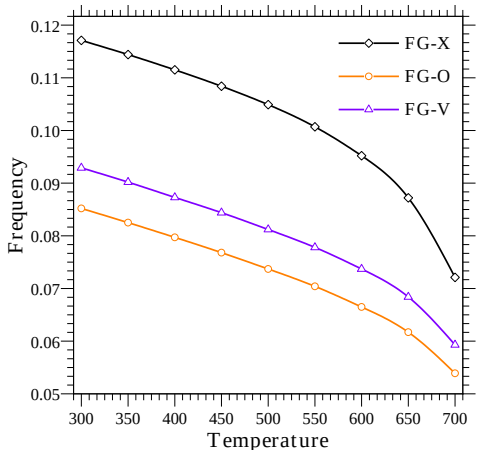

Fig. 19 Effect of temperature on dimensionless frequency of simply supported CNTRC laminated plate [0°/90°] $(V_{cnt}^{*} = 0.11, b/a = 1, a/h = 10, k = 1)$

and length scale parameter on dimensionless frequency of square (0°/90°) CNTRC laminated nanoplates using various boundary conditions is plotted in Fig. 20. It is also noticed from this figure that the dimensionless frequencies decrease by increasing of nonlocal parameter and by decreasing of length scale parameter.

5. Conclusions

In this research, a new four-unknowns quasi-3D higher-order shear deformation plate theory is built upon the classical plate theory to analyse the mechanical response of cross-ply nonlocal strain gradient CNTRC laminated nanoplates. Four unknowns are used here to define the displacement field of the plate. Three different pattern distributions of CNTs reinforcement along the thickness of the plate are presented in this work based on power-law function. Galerkin method is developed to solve governing equilibrium equations of the CNTRC laminated nanoplate and get closed form solutions for bending deflection, critical buckling loads and vibration frequencies. The main conclusions and observations can be summarized as:

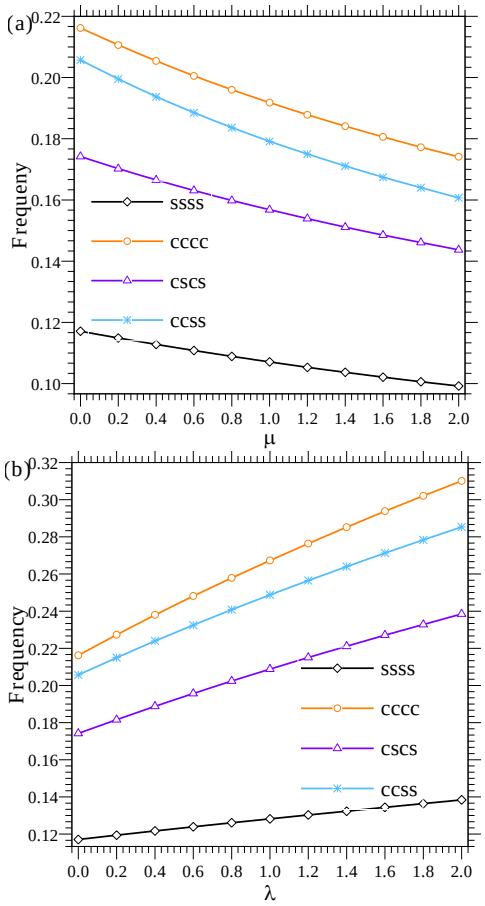

Fig. 20 Effect of nonlocal parameter and length scale parameter on dimensionless frequency of square [0°/90°] CNTRC laminated plate $(V_{cnt}^{*} = 0.11, a/h = 10, k = 1)$

• The results show that the present theory is in close agreement with Reddy's shear deformation theory.

• The stiffness of the CNTRC laminated nanoplate can be improved by using the multilayer structures, therefore increasing the critical buckling loads and frequencies and decreasing the bending deflections.

• The power-law index has a significant effect on the response of the CNTRC laminated nanoplates.

• The integration of nonlocal parameter leads to reduction of the stiffness of the nanoplate, therefore augmentation in transverse displacements and decrement in frequencies and buckling loads, while the opposite is produces when increasing length-scale parameter.

• The inclusion of temperature reduces the stiffness of the CNTRC laminated nanoplate, the bending deflections increase and the frequencies and buckling loads decrease.

Generally, the proposed analytical solution based on nonlocal strain gradient HSDT presented here affords benchmark results, that can be exploited for the evaluation of various solution procedures such as the finite-element method.

Acknowledgments

This project was funded by the Deanship of Scientific Research (DSR) at King Abdulaziz University, Jeddah,

under Grant no. G-111-135-1442. The authors, therefore, acknowledge with thanks DSR for technical and financial support.

References

Al-Furjan, M.S.H., Habibi, M., rahimi, A., Chen, G., Safarpour, H. and Tounsi, A. (2020), "Chaotic simulation of the multi-phase reinforced thermo-elastic disk using GDQM", *Eng. Comput*., 1-24. https://doi.org/10.1007/s00366-020-01144-2.

Askes, H. and Aifantis, E.C. (2009), "Gradient elasticity and flexural wave dispersion in carbon nanotubes", *Phys. Rev.* B, **80**(19), 195412. https://doi.org/10.1103/PhysRevB.80.195412.

Bekhadda, A., Cheikh, A., Bensaid, I., Hadjoui, A. and Daikh, A.A. (2019), "A novel first order refined shear-deformation beam theory for vibration and buckling analysis of continuously graded beams", *Adv. Aircr. Spacecr. Sci.*, **6**(3), 189-206. https://doi.org/10.12989/aas.2019.6.3.189.

Belarbi, M.O., Houari, M.S.A., Daikh, A.A., Garg, A., Merzouki, T., Chalak, H.D. and Hirane, H. (2021), "Nonlocal finite element model for the bending and buckling analysis of functionally graded nanobeams using a novel shear deformation theory", *Compos. Struct.*, **264**, 113712. https://doi.org/10.1016/j.compstruct.2021.113712.

Belarbi, O.M., Houari, M.S.A., Hirane, H. and Daikh, A.A. (2020). "An efficient nonlocal finite element model for the bending and buckling analysis of functionally graded nanobeams using a novel parabolic shear deformation theory", *Compos. Struct*., **264**, 113712. https://doi.org/10.1016/j.compstruct.2021.113712.

Bensaid, I. (2017), "A refined nonlocal hyperbolic shear deformation beam model for bending and dynamic analysis of nanoscale beams", *Adv. Nano Res.*, **5**(2), 113-126. http://doi.org/10.12989/anr.2017.5.2.113.

Bensaid, I., Daikh, A.A. and Drai, A. (2020), "Size-dependent free vibration and buckling analysis of sigmoid and power law functionally graded sandwich nanobeams with microstructural defects", *Proceedings of the Institution of Mechanical Engineers, Part C: Journal of Mechanical Engineering Science*, **234**(18), 3667-3688. https://doi.org/10.1177/0954406220916481.

Cao, Y., Khorami, M., Baharom, S., Assilzadeh, H. and Dindarloo, M.H. (2021), "The effects of multi-directional functionally graded materials on the natural frequency of the doubly-curved nanoshells", *Compos. Struct.*, **258**, 113403. https://doi.org/10.1016/j.compstruct.2020.113403.

Chi, S.H. and Chung, Y.L. (2006), "Mechanical behavior of functionally graded material plates under transverse load—Part I: Analysis", *Int. J. Solid Struct.*, **43**(13), 3657-74. https://doi.org/10.1016/j.ijsolstr.2005.04.011.

Daikh, A.A. (2019), "Temperature dependent vibration analysis of functionally graded sandwich plates resting on Winkler/ Pasternak/Kerr foundation", *Mater. Res. Express*., **6**, 065702. https://doi.org/10.1088/2053-1591/ab097b.

Daikh, A.A. (2020), "Thermal buckling analysis of functionally graded sandwich cylindrical shells", *Adv. Aircr. Spacecr. Sci.*, **7**(4), 335-351. http://doi.org/10.12989/aas.2020.7.4.335.

Daikh, A.A. and Megueni, A. (2018), "Thermal buckling analysis of functionally graded sandwich plates", *J. Therm. Stress*, **41**(2), 139-159. https://doi.org/10.1080/01495739.2017.1393644.

Daikh, A.A. and Zenkour, A.M., (2019), "Free vibration and buckling of porous power-law and sigmoid functionally graded sandwich plates using a simple higher-order shear deformation theory", *Mat. Res. Express*., **6**(11), 115707. https://doi.org/10.1088/2053-1591/ab48a9.

Daikh, A.A. and Zenkour, A.M. (2020), "Bending of functionally graded sandwich nanoplates resting on pasternak foundation under different boundary conditions", *J. Appl. Computat. Mech*., **6**, 1245-1259. https://doi.org/10.22055/JACM.2020.33136.2166.

Daikh, A.A., Houari, M.S.A and Tounsi, A. (2019a), "Buckling analysis of porous FGM sandwich nanoplates due to heat conduction via nonlocal strain gradient theory", *Eng. Res. Express*., **1**, 015022. https://doi.org/10.1088/2631-8695/ab38f9.

Daikh, A.A., Guerroudj, M., Elajrami, M. and Megueni, A. (2019b), "Thermal buckling of functionally graded sandwich beams", *Adv. Mater. Res.*, **1156**, 43-59. https://doi.org/10.4028/www.scientific.net/AMR.1156.43.

Daikh, A.A., Bachiri, A., Houari, M.S.A. and Tounsi. (2020a), "Size dependent free vibration and buckling of multilayered carbon nanotubes reinforced composite nanoplates in thermal environment", *Mech. Based Des. Struct.*, 1-29. https://doi.org/10.1080/15397734.2020.1752232.

Daikh, A.A., Houari, M.S.A. and Eltaher. M.A. (2020b), "A novel nonlocal strain gradient Quasi-3D bending analysis of sigmoid functionally graded sandwich nanoplates", *Compos. Struct.*, 113347. https://doi.org/10.1016/j.compstruct.2020.113347.

Daikh, A.A., Drai, A., Bensaid, I., Houari, M.S.A. and Tounsi A. (2020c), "On vibration of functionally graded sandwich nanoplates in the thermal environment", *J. Sandw. Struct. Mater*., 1-28. https://doi.org/10.12989/aas.2020.7.4.335.

Daikh, A.A., Drai, A., Houari M.S.A. and Mohamed A. Eltaher. (2020d), "Static analysis of multilayer nonlocal strain gradient nanobeam reinforced by carbon nanotubes", *Steel Compos. Struct.*, **36** (6), 643-656. https://doi.org/10.12989/scs.2020.36.6.643.

Daikh, A.A., Bensaid, I., Bachiri, A., Houari, M.S.A. Tounsi, A. and Merzouki, T. (2020e), "On static bending of multilayered carbon nanotube-reinforced composite plates", *Comput. Concrete.*, **26**(2), 137-150. https://doi.org/10.12989/cac.2020.26.2.137.

Daikh, A.A., Bensaid, I. and Zenkour, A.M. (2020f), "Temperature dependent thermomechanical bending response of functionally graded sandwich plates", *Eng. Res. Express*., **2**, 015006. https://doi.org/10.1088/2631-8695/ab638c.

Daikh, A.A., Houari, M.S.A., Belarbi, M.O. Chakraverty, S. and Eltaher, M.A. (2021), "Analysis of axially temperature-dependent functionally graded carbon nanotube reinforced composite plates", *Eng. Comput*., 1-22. https://doi.org/10.1007/s00366-021-01413-8.

Duc, N.D., Lee, J., Nguyen-Thoi, T. and Pham, T.T. (2017), "Static response and free vibration of functionally graded carbon nanotube-reinforced composite rectangular plates resting on Winkler-Pasternak elastic foundations", *Aerosp. Sci. Technol.*, **68**, 391-402. https://doi.org/10.1016/j.ast.2017.05.032.

Ebrahimi, F. and Barati, A.F. (2016), "Analytical solution for nonlocal buckling characteristics of higher-order inhomogeneous nanosize beams embedded in elastic medium", *Adv. Nano Res.*, **4**(3), 229-249. http://doi.org/10.12989/anr.2016.4.3.229.

Ehyaei, J., Akbarshahi, A., and Shafiei, N. (2017), "Influence of porosity and axial preload on vibration behavior of rotating FG nanobeam", *Adv. Nano Res.*, **5**(2), 141-169. http://doi.org/10.12989/anr.2017.5.2.141.

Ekinci, K. and Roukes, M. (2005), "Nanoelectromechanical systems", *Rev. Sci. Instrum.*, **76**(6), 061101. https://doi.org/10.1063/1.1927327.

Eltaher, M.A., Khater, M.E., Park, S., Abdel-Rahman, E. and Yavuz M. (2016), "On the static stability of nonlocal nanobeams using higher-order beam theories", *Adv. Nano Res.*, **4**(1), 51-64. http://doi.org/10.12989/anr.2016.4.1.051.

Eringen, A.C. (1972), "Nonlocal polar elastic continua", *Int. J. Eng. Sci.*, **10**(1), 1-16.

https://doi.org/10.1016/0020-7225(72)90070-5.
Eringen, A.C. (1983), "On differential equations of nonlocal elasticity and solutions of screw dislocation and surface waves", *J. Appl. Phys.*, **54**(9), 4703-10. https://doi.org/10.1063/1.332803.
Esawi, A.M. and Farag, M.M. (2007), "Carbon nanotube reinforced composites: Potential and current challenges", *Mater. Des.*, **28**(9), 2394-401. https://doi.org/10.1016/j.matdes.2006.09.022.
Esen, I., Abdelrahman, A.A. and Eltaher, Mohamed A. (2020), "Dynamics analysis of timoshenko perforated microbeams under moving loads", *Eng. Comput*., 1-17. https://doi.org/10.1007/s00366-020-01212-7.
Esen, I., Abdelrahman, A.A. and Eltaher, M.A. (2021), "Free vibration of a cracked FG microbeam embedded in an elastic matrix and exposed to magnetic field in a thermal environment", *Compos. Struct*., **261**, 113552/ https://doi.org/10.1016/j.compstruct.2021.113552.
Esen, I., Daikh, A.A. and Eltaher, M.A. (2021), "Dynamic response of nonlocal strain gradient FG nanobeam reinforced by carbon nanotubes under moving point load", *Eur. Phys. J. Plus.*, **136**, 458. https://doi.org/10.1140/epjp/s13360-021-01419-7.
Ferreira, A., Castro, L.M. and Bertoluzza, S. (2008), "A high order collocation method for the static and vibration analysis of composite plates using a first-order theory", *Compos. Struct.*, **89**(3), 424-32. https://doi.org/10.1016/j.compstruct.2008.09.006.
Gurtin, M.E. and Murdoch, A.I. (1978), "Surface stress in solids", *Int. J. Solid Struct.*, **197**(14), 431-440. https://doi.org/10.1016/0020-7683(78)90008-2.
Hamed, M.A. Abo-bakr, R.M. Mohamed, S.A. and Eltaher, M.A. (2020), "Influence of axial load function and optimization on static stability of sandwich functionally graded beams with porous core", *Eng. Comput.*, **6**, 1929-1946. https://doi.org/10.1007/s00366-020-01023-w.
Han, Y. and Elliott, J. (2007) , "Molecular dynamics simulations of the elastic properties of polymer/carbon nanotube composites", *Computat. Mater. Sci.*, **39**(2), 315-323. https://doi.org/10.1016/j.commatsci.2006.06.011.
Harris, P.J. (2004), "Carbon nanotubes and related structures: new materials for the twenty-first century", *Am. Assoc. Phys. Teach.*, **72**(3), 415. https://doi.org/10.1017/CBO9780511605819.
Houari M.S.A, Tounsi, A. Bessaim, A. and Mahmoud, S.R. (2016), "A new simple three-unknown sinusoidal shear deformation theory for functionally graded plates", *Steel Compos. Struct.*, **22**(2), 257-276. http://doi.org/10.12989/scs.2016.22.2.257.
Houari, M.S.A., Tounsi, A. and Bég, O.A. (2013), "Thermoelastic bending analysis of functionally graded sandwich plates using a new higher order shear and normal deformation theory", *Int. J. Mech. Sci.*, **76**, 102-11. https://doi.org/10.1016/j.ijmecsci.2013.09.004.
Hussain, M., Naeem, M. N. and Tounsi, A. (2020a), "Response of orthotropic Kelvin modeling for single-walled carbon nanotubes: Frequency analysis", *Adv. Nano Res.*, **8**(3), 229-244. https://doi.org/10.12989/anr.2020.8.3.229.
Hussain, M., Naeem, M. N., Asghar, S., & Tounsi, A. (2020b), "Theoretical impact of Kelvin's theory for vibration of double walled carbon nanotubes", *Adv. Nano Res.*, **8**(4), 307-322. https://doi.org/10.12989/anr.2020.8.4.307.
Jena, S.K., Chakraverty, S. and Tornabene, F. (2019), "Dynamical behavior of nanobeam embedded in constant, linear, parabolic and sinusoidal types of Winkler elastic foundation using first-Order nonlocal strain gradient model", *Mater. Res. Express*., **6**, 0850f2. https://doi.org/10.1088/2053-1591/ab2779.
Liew, K.M. and Alibeigloo, A. (2020) , "Predicting bucking and vibration behaviors of functionally graded carbon nanotube reinforced composite cylindrical panels with three-dimensional flexibilities", *Compos. Struct*., 113039. https://doi.org/10.1016/j.compstruct.2020.113039.
Lim, C.W., Zhang, G. and Reddy, J.N. (2015), "A higher-order nonlocal elasticity and strain gradient theory and its applications in wave propagation", *J. Mech. Phys. Solid*, **78**, 298-313. https://doi.org/10.1016/j.jmps.2015.02.001
Lu, L., She, G.L. and Guo, X. (2021a), "Size-dependent postbuckling analysis of graphene reinforced composite microtubes with geometrical imperfection", *Int. J. Mech. Sci*., **199**, 106428. https://doi.org/10.1016/j.ijmecsci.2021.106428.
Lu, L., Wang, S., Li, M. and Guo, X. (2021b), "Free vibration and dynamic stability of functionally graded composite microtubes reinforced with graphene platelets", *Compos. Struct*., **272**(15), 114231. https://doi.org/10.1016/j.compstruct.2021.114231.
Mantari, J. and Ore, M. (2015), "Free vibration of single and sandwich laminated composite plates by using a simplified FSDT", *Compos. Struct.*, **132**, 952-959. https://doi.org/10.1016/j.compstruct.2015.06.035.
Neves, A., Ferreira, A., Carrera, E., Cinefra, M., Roque, C.M.C., Jorge, R.M.N. and Soares, C.M.M. (2013), "Free vibration analysis of functionally graded shells by a higher-order shear deformation theory and radial basis functions collocation, accounting for through-the-thickness deformations", *Eur. J. Mech. A Solid*, **37**, 24-34. https://doi.org/10.1016/j.euromechsol.2012.05.005.
Nguyena, T.N., Ngo, T.D. and Nguyen-Xuan, H. (2017), "A novel three-variable shear deformation plate formulation: Theory and Isogeometric implementation", *Comput. Methods Appl. Mech. Eng*., **326**, 376-401. http://doi.org/10.1016/j.cma.2017.07.024.
Nguyena, T.N., Thai, C.H., Luu, A.T., Nguyen-Xuan, H. and Lee, J. (2019), "NURBS-based postbuckling analysis of functionally graded carbon nanotube-reinforced composite shells", *Comput. Method Appl. M*., **347**, 983-1003. https://doi.org/10.1016/j.cma.2019.01.011.
Nguyen-Xuan, H., Thai, C.H. and Nguyen-Thoi T. (2013), "Isogeometric finite element analysis of composite sandwich plates using a higher order shear deformation theory", *Compos. Part B Eng.*, **55**, 558-74. https://doi.org/10.1016/j.compositesb.2013.06.044.
Reddy, J.N. (1984), "A simple higher-order theory for laminated composite plates", *J. Appl. Mech.*, **51**, 745-752. https://doi.org/10.1115/1.3167719.
Shahsavari, D., Karami, B. and Mansouri S. (2018), "Shear buckling of single layer graphene sheets in hygrothermal environment resting on elastic foundation based on different nonlocal strain gradient theories", *Eur. J. Mech. A Solid*, **67**, 200-214. https://doi.org/10.1016/j.euromechsol.2017.09.004.
She, G.L., Liu, H.B. and Karami, B. (2021), "Resonance analysis of composite curved microbeams reinforced with graphene nanoplatelets", *Thin Wall. Struct*., **160**, 107407. https://doi.org/10.1016/j.tws.2020.107407.
She, G.L., Yuan, F.G., Ren, Y.R., Liu, H.B and Xiao, W.S. (2018), "Nonlinear bending and vibration analysis of functionally graded porous tubes via a nonlocal strain gradient theory", *Compos. Struct.*, **203**, 614-623. https://doi.org/10.1016/j.compstruct.2018.07.063.
Shen, H.S. (2009), "Nonlinear bending of functionally graded carbon nanotube-reinforced composite plates in thermal environments", *Compos. Struct.*, **91**(1), 9-19. https://doi.org/10.1016/j.compstruct.2009.04.026.
Singh, D.B. and Singh, B.N. (2017), "New higher order shear deformation theories for free vibration and buckling analysis of laminated and braided composite plates", *Int. J. Mech. Sci.*, **131**, 265-277. https://doi.org/10.1016/j.ijmecsci.2017.06.053.
Soldatos, K.P. (1992), "A transverse shear deformation theory for

homogeneous monoclinic plates", *Acta. Mech.*, **94**(3-4), 195-220. https://doi.org/10.1007/BF01176650.

Thai, C.H., Kulasegaram, S., Tran, L.V. and Nguyen-Xuan, H. (2014), "Generalized shear deformation theory for functionally graded isotropic and sandwich plates based on isogeometric approach", *Comput. Struct.*, **141**, 94-112. http://doi.org/10.1016/j.compstruc.2014.04.003.

Thai, C.H., Ferreira, A., Bordas, S. and Rabczuk, T. (2013), "Nguyen-Xuan H. Isogeometric analysis of laminated composite and sandwich plates using a new inverse trigonometric shear deformation theory", *Eur. J. Mech. A Solid*, **43**, 89-108. https://doi.org/10.1016/j.euromechsol.2013.09.001.

Thai, C.H., Zenkour, A.M., Wahab, M.A. and Nguyen-Xuan, H. (2016), "A simple four-unknown shear and normal deformations theory for functionally graded isotropic and sandwich plates based on isogeometric analysis", *Compos. Struct.*, **139**, 77-95. https://doi.org/10.1016/j.compstruct.2015.11.066.

Thai, H.T., Nguyen, T.K., Vo, T.P., Lee, J. (2014), "Analysis of functionally graded sandwich plates using a new first-order shear deformation theory", *Eur. J. Mech. A Solid*, **45**, 211-25. https://doi.org/10.1016/j.euromechsol.2013.12.008.

Thang, P.T., Tran, P. and Nguyen-Thoi, T. (2021), "Applying nonlocal strain gradient theory to size-dependent analysis of functionally graded carbon nanotube-reinforced composite nanoplates" *Appl. Math. Modell.*, **93**, 775-791. https://doi.org/10.1016/j.apm.2021.01.001.

Touloukian, Y.S. (1967), *Thermophysical Properties of High Temperature Solid Materials*, MacMillan, New York, U.S.A.

Touratier M. (1991), "An efficient standard plate theory", *Int. J. Eng. Sci.*, **29**(8), 901-916. https://doi.org/10.1016/0020-7225(91)90165-Y.

Vaghefi, R. (2020), "Thermo-elastoplastic analysis of functionally graded sandwich plates using a three-dimensional meshless model", *Compos. Struct.*, **242**, 112144. https://doi.org/10.1016/j.compstruct.2020.112144.

Vuong, P.M. and Duc, N.D. (2020), "Nonlinear buckling and post-buckling behavior of shear deformable sandwich toroidal shell segments with functionally graded core subjected to axial compression and thermal loads", *Aerosp. Sci. Technol.*, **106**, 106084. https://doi.org/10.1016/j.ast.2020.106084.

Wattanasakulpong, N., Chaikittiratana, A. (2015, "Exact solutions for static and dynamic analyses of carbon nanotube-reinforced composite plates with Pasternak elastic foundation", *Appl. Math. Modell.*, **39**, 5459-5472. https://doi.org/10.1016/j.apm.2014.12.058

Yang, F., Chong, A., Lam, D.C.C. and Tong, P. "Couple stress based strain gradient theory for elasticity", *Int. J. Solid Struct.*, **39**(10), 2731-2743. https://doi.org/10.1016/S0020-7683(02)00152-X.

Zenkour, A.M. (2016), "Buckling of a single-layered graphene sheet embedded in visco-Pasternak", *Adv. Nano Res.*, **4**(4), 309-329. http://doi.org/10.12989/anr.2016.4.4.309.

Zhang, Y.Y., Wang, X.Y., Zhang, X., Shen, H.M. and She, G.L. (2021), "On snapbuckling of FG-CNTR curved nanobeams considering surface effects", *Steel Compos. Struct.*, **38**(3), 293-304. https://doi.org/10.12989/scs.2021.38.3.293.